Received: 12 May 2023 | Revised: 27 September 2023 | Accepted: 30 September 2023

DOI: 10.1002/pro.4818

RESEARCH ARTICLE

THE PROTEIN SOCIETY WILEY

Integrative modeling of guanylate binding protein dimers

Wibke Schumann[1,2] | **Jennifer Loschwitz**[1,2] | **Jens Reiners**[3] | **Daniel Degrandi**[4] | **Larissa Legewie**[4] | **Kai Stühler**[5,6] | **Klaus Pfeffer**[4] | **Gereon Poschmann**[5] | **Sander H. J. Smits**[3,7] | **Birgit Strodel**[1,2]

[1]Institute of Theoretical and Computational Chemistry, Heinrich Heine University Düsseldorf, Düsseldorf, Germany

[2]Institute of Biological Information Processing: Structural Biochemistry, Forschungszentrum Jülich, Jülich, Germany

[3]Center for Structural Studies, Heinrich Heine University Düsseldorf, Düsseldorf, Germany

[4]Institute of Medical Microbiology and Hospital Hygiene, Heinrich Heine University, Düsseldorf, Germany

[5]Institute of Molecular Medicine, Proteome Research, Medical Faculty and University Hospital Düsseldorf, Heinrich Heine University Düsseldorf, Düsseldorf, Germany

[6]Molecular Proteomics Laboratory, Biomedical Research Centre (BMFZ), Heinrich Heine University Düsseldorf, Düsseldorf, Germany

[7]Institute for Biochemistry, Heinrich Heine University Düsseldorf, Düsseldorf, Germany

Correspondence
Birgit Strodel, Institute of Theoretical and Computational Chemistry, Heinrich Heine University Düsseldorf, 40225 Düsseldorf, Germany.
Email: b.strodel@fz-juelich.de

Funding information
Deutsche Forschungsgemeinschaft (DFG, German Research Foundation), Grant/Award Numbers: INST 208/761-1 FUGG, 417919780; Jürgen Manchot Promotionsstipendium; Gauss Centre for Supercomputing e.V.

Abstract

Guanylate-binding proteins (GBPs) are essential interferon-γ-activated large GTPases that play a crucial role in host defense against intracellular bacteria and parasites. While their protective functions rely on protein polymerization, our understanding of the structural intricacies of these multimerized states remains limited. To bridge this knowledge gap, we present dimer models for human GBP1 (hGBP1) and murine GBP2 and 7 (mGBP2 and mGBP7) using an integrative approach, incorporating the crystal structure of hGBP1's GTPase domain dimer, crosslinking mass spectrometry, small-angle X-ray scattering, protein–protein docking, and molecular dynamics simulations. Our investigation begins by comparing the protein dynamics of hGBP1, mGBP2, and mGBP7. We observe that the M/E domain in all three proteins exhibits significant mobility and hinge motion, with mGBP7 displaying a slightly less pronounced motion but greater flexibility in its GTPase domain. These dynamic distinctions can be attributed to variations in the sequences of mGBP7 and hGBP1/mGBP2, resulting in different dimerization modes. Unlike hGBP1 and its close ortholog mGBP2, which exclusively dimerize through their GTPase domains, we find that mGBP7 exhibits three equally probable alternative dimer structures. The GTPase domain of mGBP7 is only partially involved in its dimerization, primarily due to an accumulation of negative charge, allowing mGBP7 to dimerize independently of GTP. Instead, mGBP7 exhibits a strong

Wibke Schumann and Jennifer Loschwitz contributed equally to this work.

Reviewing Editor: Nir Ben-Tal

tendency to dimerize in an antiparallel arrangement across its stalks. The results of this work go beyond the sequence–structure–function relationship, as the sequence differences in mGBP7 and mGBP2/hGBP1 do not lead to different structures, but to different protein dynamics and dimerization. The distinct GBP dimer structures are expected to encode specific functions crucial for disrupting pathogen membranes.

KEYWORDS

crosslinking mass spectrometry, guanylate binding proteins, MD simulation, protein–protein docking, sequence–structure–function relationship, small angle x-ray scattering

1 | INTRODUCTION

Dynamin superfamily proteins (DSPs) are mechanochemical enzymes, converting GTPase activity into some of the highest torques observed for proteins, which is then used for membrane fusion or fission (Ford & Chappie, 2019; Morlot et al., 2012). In contrast to the smaller Rat sarcoma virus (Ras)-like GTPases, DSPs exhibit lower substrate affinity but higher basal hydrolysis rates, which is highly stimulated upon oligomerization (Ghosh et al., 2006). Multimers of DSPs form ordered rings, lattices, or helices, thereby tubulating membranes (Ford & Chappie, 2019), and are thus involved in critical cellular functions, such as endocytosis, mitochondrial membrane tubulation, cell division, and vesiculation (Gao & Hu, 2021; Praefcke & McMahon, 2004). As some of the DSPs have been studied separately, the nomenclature of domains is not unified, although they are functionally homologous and feature a modular composition of domains. Some examples are depicted in Figure 1a. The approximately 300 amino acid-long GTPase domain (G domain) is the only domain conserved at the sequence level and always exhibits the typical motifs of a nucleotide-binding domain (motifs G1–G5). GTPase activity, although stimulated by multimerization, is usually not dependent upon it (Stowell et al., 1999; Warnock et al., 1996). Other domains of DSPs are structurally conserved, even if they are not homologous in sequence. The bundle signaling element (BSE or neck or helical bundle 1) is an elongated helical domain that is in contact with the G domain via the so-called hinge 2 and connects to the stalk (or trunk or middle/effector-domain or helical bundle 2) domain via hinge 1. The membrane interaction can be mediated by a pleckstrin homology (PH) domain, the L4 loop, a variable domain (VD), a paddle or a C-terminal region (Figure 1a,b) (Ford & Chappie, 2019).

One subfamily of DSPs is the guanylate binding protein family (GBPs, Figure 1b), which is known, among others, for their anti-*Toxoplasma gondii* (Degrandi et al., 2007, 2013; Steffens et al., 2020; Taylor et al., 2004), anti-HIV (Krapp et al., 2016), and anti-*Chlamydia trachomatis* (Lindenberg et al., 2017; Xavier et al., 2020) activity. Using bioinformatic/phylogenetic methods, seven human GBPs (hGBP1 to hGBP7) and 11 murine GBPs (mGBP1 to mGBP11) have been identified (Degrandi et al., 2007; Olszewski et al., 2006). The GBPs contain three domains (Figure 1b,c): (1) the G domain for GTP binding and hydrolysis (Figure 1d), (2) a middle domain (M domain) for regulation, and (3) a GTP effector domain (E domain) for interactions with lipid membranes. The latter two domains can be considered together as the M/E domain. In this work, we focus on hGBP1, mGBP2, and mGBP7, which are therefore presented in more detail below. The E domain of hGBP1 and mGBP2 contains a C-terminal CaaX motif that, after posttranslational modification, leads to an isoprenyl lipid anchor. In mGBP7, on the other hand, the E domain contains an extended C terminus (called the CT tail) that includes approximately 50 other residues that have been shown to be essential for membrane binding of the protein (Figure 1b,c) (Legewie et al., 2019). The mGBP2, the murine counterpart of the extensively studied hGBP1 with a notable sequence identity of 66.2% (see Table S1), and mGBP7 both play a central role in defense against *T. gondii*. Their defense mechanism involves binding to the membrane of the parasitophorous vacuole of *T. gondii*. Remarkably, the membrane of this vacuole is composed of lipids from the host cell, thus hiding the parasite from the host cell defense response. It is noteworthy that mGBP2 binds to this membrane before mGBP7, while the absence of mGBP7 results in higher mortality in mice infected with the parasite than deletion of mGBP2 (Degrandi et al., 2013; Steffens et al., 2020). Furthermore, GBPs alternate between monomeric, dimeric, and polymeric states, with the polymeric configuration including thousands of GBPs on the parasite-related membranes (Kravets et al., 2016; Shydlovskyi et al., 2017; Zhu et al., 2021). Nucleotides are required for the oligomerization of most DSPs. This is also true for the dimerization of hGBP1 and mGBP2, which is largely

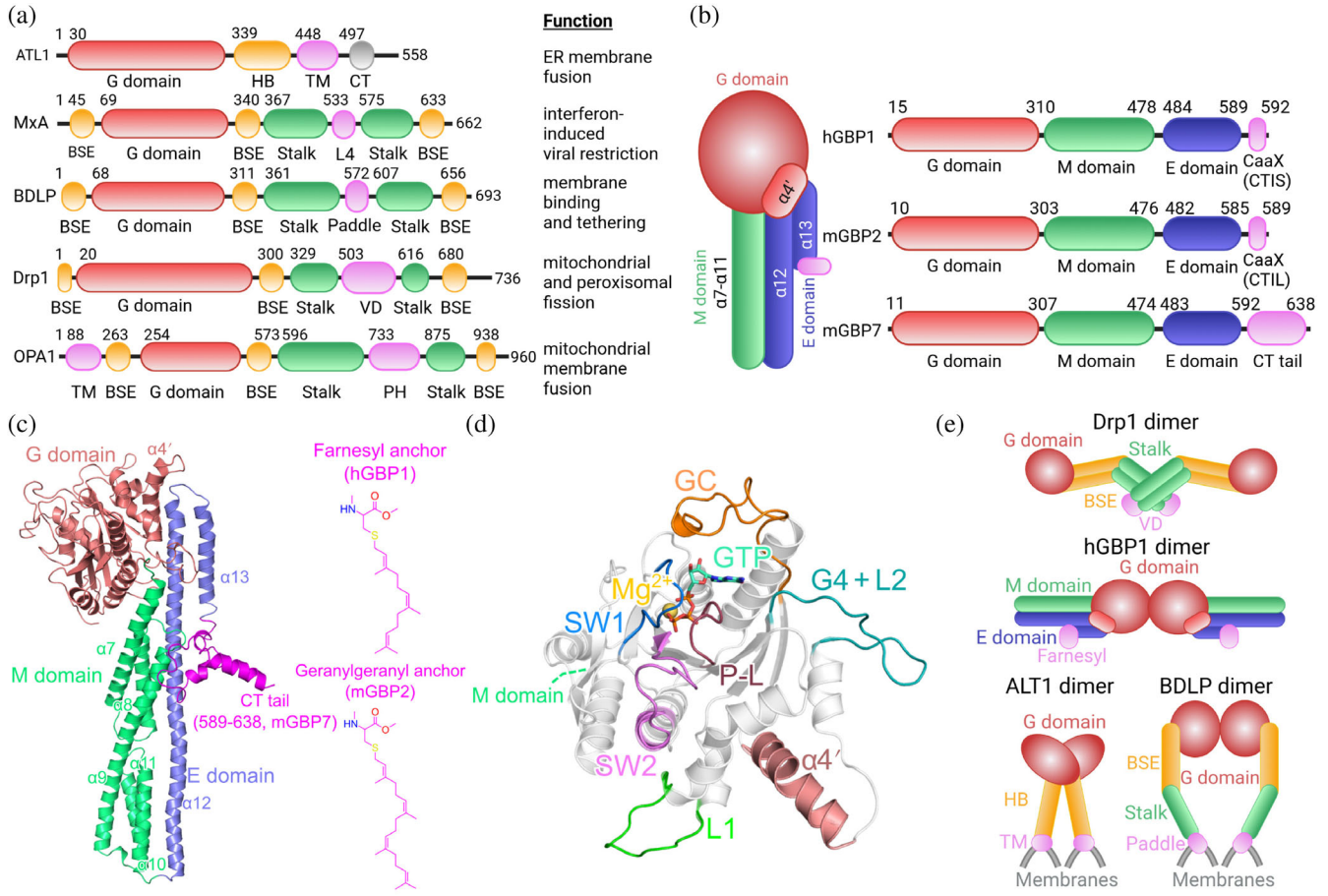

FIGURE 1 Structural organization and dimerization modes of dynamin superfamily proteins (DSPs) and guanylate-binding proteins (GBPs). (a) Schematic domain organization of selected DSPs: atlastin 1 (ATL1), myxovirus resistance protein 1 (MxA), BDLP, dynamin-related protein 1 (Drp1), OPA1 (from optic atrophy gene 1) (Ford & Chappie, 2019; Gao & Hu, 2021; Yu et al., 2020). DSPs exhibit a highly conserved large GTPase domain (G domain, red), a structural element or domain for membrane binding (violet) which can be a transmembrane (TM) domain, the L4 loop of the G domain, a paddle domain, a variable (VD) domain, or a pleckstrin homology (PH) domain, two elongated α-helical bundle domains called stalk (green), and a bundle signaling element/helical bundle (BSE/HB, orange). The function of each DSP is given on the right. (b) Schematic domain organization of GBPs. They are split into three domains: the large GTPase (G) domain (red), the middle (M) domain (green), and the effector (E) domain (blue), followed by a region responsible for membrane binding. It is either a CaaX box for isoprenylation or an elongated C-terminal (CT) tail. (c) The structure of mGBP7 is shown as cartoon. The helices discussed in this work (α4′, α7–13) are indicated. At the C-terminus, mGBP7 features a helical CT tail, while human GBP1 (hGBP1) and murine GBP2 (mGBP2) become isoprenylated with either a farnesyl (hGBP1) or a geranylgeranyl (mGBP2) group (2D structures on the right). (d) Close-up of the G domain of mGBP7. The four conserved GTP binding site motifs and other important structural elements are highlighted: P-loop (P-L) or G1 (dark red), G2 (also called switch1 (SW1), blue), G3 (also called switch2 (SW2), magenta), G4 plus loop L2 (G4 + L2, turquoise), loop L1 (green), guanine cap (GC, red), and α4′ (red). The bound nucleotide GTP is shown with sticks and colored by atom type and Mg^{2+} is shown as a yellow sphere. (e) Known DSP dimerization modes are shown for Drp1 (Protein Data Bank [PDB] ID 4BEJ) (Fröhlich et al., 2013), hGBP1 (PDB ID 2BC9) (Ghosh et al., 2006) featuring the G domain dimer (Ford & Chappie, 2019), ATL1 (PDB ID 3Q5D) (Byrnes & Sondermann, 2011), and BDLP (PDB ID 2W6D) (Low et al., 2009). In general, the dimerization occurs via the stalk regions (Drp1) or via the G domains (ATL1, hGBP1, and BDLP). Panels (a), (b), and (e) were created with BioRender.

dependent on nucleotide binding, while mGBP7 can form dimers in the absence of GTP (Kravets et al., 2012; Legewie et al., 2019; Prakash et al., 2000). Nucleotide-independent oligomerization has also been found for optic atrophy gene 1 (OPA1; Figure 1a) (Yu et al., 2020). A characteristic of GBPs as opposed to other DSPs is that they are able to hydrolyze GDP further to GMP, where the second hydrolysis step was shown to take place in a polymerized state (Britzen-Laurent et al., 2010; Ince et al., 2017). Upon GTP shortage, these polymers dissociate, indicating that GMP cannot stabilize the polymer (Sistemich et al., 2020).

Concerning the structural details of polymerized DSPs, the available information primarily pertains to dimers. Dimer structures of DSPs that are deposited in the Protein Data Bank (PDB) display G domain dimers

(hGBP1 [Ghosh et al., 2006], Irga6 [Schulte et al., 2016], dynamin [Chappie et al., 2010]), crossed-stalk dimers (dynamin [Faelber et al., 2011]), and parallel stalk dimers (bacterial dynamin like protein [BDLP; Low et al., 2009; Low & Löwe, 2006], Sey1p [Yan et al., 2015]) (Figure 1e), while higher-order oligomers combine several of these interfaces (Reubold et al., 2015). Thus far, only three partial dimer structures of GBPs are available (Cui et al., 2021; Ghosh et al., 2006). The structure by Ghosh et al. (Ghosh et al., 2006) is a dimer only formed by the G domains of hGBP1, while in the partial hGBP1 and hGBP5 dimer structures reported by others the G and M domains (the E domain is missing) interact lengthwise (Cui et al., 2021; Kuhm et al., 2023; Weismehl et al., 2023). However, in either case the protein–protein interaction is mainly mediated via the same G domain interaction motif. Such coexistence of different dimerization modes was also demonstrated for atlastin (Bian et al., 2011; Byrnes & Sondermann, 2011). The primary objective of this study is to examine the structures and dynamics of mGBP2 and mGBP7 dimers. To achieve this goal, we leverage the high sequence similarity between mGBP2 and hGBP1. Additionally, we employ protein–protein docking to create a structural model for the mGBP2 dimer. For mGBP7, we utilize a combination of protein–protein docking, small-angle x-ray scattering (SAXS), and crosslinking mass spectrometry (XL-MS) to establish potential dimer structures. We evaluate the stability of these dimer models through molecular dynamics (MD) simulations, allowing us to compare GBP monomers (Barz et al., 2019; Loschwitz et al., 2023) and dimers while identifying critical residues at the dimerization interfaces. Our findings suggest that mGBP7 exhibits distinct dimerization preferences compared to hGBP1 and mGBP2, in line with variations in their sequences and dynamics. This research represents a significant step toward our overarching objective, which is to comprehend the functioning of membrane-bound GBP multimers. Understanding the structures and dynamics of the smallest organizational subunits is vital to achieving this long-term goal.

2 | RESULTS

2.1 | Sequence comparison of hGBP1, mGBP2, and mGBP7

We begin our study with a comparative analysis of the sequences of hGBP1, mGBP2, and mGBP7 and identify correlations between variations in their sequences and differences in their biochemical characteristics. As will be shown below, some of the sequence differences are also relevant to differences in their dimerization. The most relevant sequence and biochemical properties are summarized in Table S1.

2.1.1 | G domain

The G domain contains the four G motifs (G1–G4) needed for the GTP hydrolysis, the guanine cap, the loop 1 (L1), and the α4′ helix (Figure 1d). The GTP binding affinity is slightly different between the proteins, with mGBP7 having the highest and hGBP1 the lowest affinity (Kravets et al., 2012; Praefcke et al., 2004). To understand the differences in the GTP binding, we aligned the sequences of the three proteins using T-Coffee (Madeira et al., 2019; Notredame et al., 2000) and analyzed their amino acid compositions in terms of physicochemical properties (Figure S1). This extends to a representation of their electrostatic potential surface (EPS) for the whole protein and the GTP binding site in particular (Figure S2). All three GBPs are rather negatively charged on one side of the protein, yet feature a mix of positive and negative charges on the opposite side, yet with a higher share of positive charges in the G domain on that protein side. Of the three proteins, mGBP7 is the most negative on either side, followed by mGBP2. The G1 motif, also called phosphate-binding or P-loop (P-L), is highly conserved and is key for GTP binding and hydrolysis. The sequences of the next two G motifs, G2 and G3 (also called switches SW1 and SW2), also feature only minor changes among the three proteins, and in particular the key residues T75 of SW1 needed for interactions with Mg^{2+} as well as S73 of SW1 and E99 of SW2 required for coordinating the nucleophilic water molecule during the hydrolysis reaction are highly conserved (Ghosh et al., 2006; Praefcke et al., 2004). The G4 motif, which is responsible for mediating nucleotide specificity together with the loop 2 (G4 + L2), is more positively charged in mGBP7 than in the other two GBPs. The most important element for dimerization of hGBP1 is the guanine cap, which is an unstructured loop region (Barz et al., 2019; Ghosh et al., 2006). In hGBP1, two arginine residues, R240 and R244 exhibit a key role in the dimerization (Wehner et al., 2012). Interestingly, mGBP7 has oppositely charged residues in that region. Examples include R244 in hGBP1 and R242 in mGBP2, which correspond to D242 in mGBP7, and K246 in hGBP1 and Q244 in mGBP2, which correspond to E244 in mGBP7 (Figure S1). As a result, the overall charge of the guanine cap in mGBP7 is while it is neutral in hGBP1 and mGBP2. The other larger loop region of the G domain is the loop 1 (L1), which in mGBP2 is more hydrophobic and polar but less charged than in hGBP1 and mGBP7. It

can therefore interact with the geranylgeranyl lipid anchor and also the helix α12 of the E domain (Loschwitz et al., 2023). The α4′ helix, which belongs to the G domain, also interacts with the α12 as well as with α13 via salt bridges, which keeps the E domain close to the G domain (Vöpel et al., 2010). For hGBP1 it was demonstrated that this "lock" can be broken by GTP hydrolysis, releasing the whole E domain from the G domain in order for hGBP1 to polymerize and tether membranes (Ince et al., 2020; Shydlovskyi et al., 2017).

2.1.2 | M/E domain

All three proteins harbor a considerable amount of charged residues in the M/E domain. A major difference is that the M domain of mGBP7 has an overall charge of +10, whereas that charge is −2 and 0 in hGBP1 and mGBP2, respectively (Figure S1). This might be of relevance for the membrane binding of mGBP7, especially as these positive charges are preferentially found on one side of the protein (Figure S2A) and are augmented by an overall positive charge of +3 of the CT tail, which was already demonstrated to be essential for membrane interaction (Legewie et al., 2019). A common feature of the three proteins is that charged residues are found in clusters. Examples are triply repeated residues of the same charge, like $^{417/419}$EEE$^{419/421}$ in mGBP2/hGBP1 and ^{439}RKK^{441} in mGBP7, as well as mixtures of positively and negatively charged residues, often in repeats, like ^{389}EKKRDD^{394} in hGBP1, ^{389}KRD^{391} in mGBP2, and ^{388}EEKRED^{393} in mGBP7. The second variant occurs more often in all three GBPs and adds stability to the long α12 due to intrahelical salt-bridge formation (Marqusee & Baldwin, 1987; Wolny et al., 2017). To be specific, α12 is 81 residues long and contains 21 (hGBP1 and mGBP7) or 30 (mGBP2) i, $i + 3$ or i, $i + 4$ combinations of oppositely charged side chains, which may form salt bridges. The helices α12/13 are not amphipathic, as the charged residues are not only solvent-exposed, but some of them are also buried (Figure S2B). For hGBP1, we showed that some of the charged residues of α12 form salt bridges with the M domain that are crucial for the stability of that long helix (Barz et al., 2019). The α13 of hGBP1 and mGBP7 exhibits clusters of positive charges, ^{582}KMRRK^{587} and ^{567}KRK^{569}, which have been shown to be required for binding to lipid membranes in addition to the farnesylation in hGBP1 (Zhu et al., 2021) and the CT tail (Legewie et al., 2019). The mGBP2 only has a single lysine residue (K585) in α13 immediately upstream of the CaaX motif, which is, however, expected to help with membrane binding together with the geranylgeranyl lipid anchor.

2.2 | Molecular dynamics of monomeric GBPs

We continue our study by comparing the dynamics of the monomers of hGBP1, mGBP2, and mGBP7, both to further elucidate the differences between the proteins and to have the monomer dynamics as a reference for the dynamics of the proteins in the oligomerized state. The dynamics of hGBP1 and mGBP2 was discussed in detail in our previous work (Barz et al., 2019; Loschwitz et al., 2023), while the dynamics of mGBP7 is being unraveled in this study. As simulation method, Hamiltonian replica exchange molecular dynamics (HREMD) was applied. The three proteins were simulated in their apo-state (denoted as [h/m]GBPn_{apo} with $n = 1$, 2, or 7) and for mGBP2 and mGBP7 we also considered the GTP-bound monomer (mGBPn_{GTP}). For hGBP1 and mGBP7 we used 30 × 400 ns MD replicas and for mGBP2 it was 16 × 200 ns MD replicas. For mGBP2, we had shown that the smaller HREMD setup was sufficient as no further protein states were sampled in a 40 × 400 ns HREMD simulation (Loschwitz et al., 2023). For the analysis, the protein conformations collected in the HREMD target replica were considered, where no changes were made to the potential energy function.

2.2.1 | Overall protein flexibility

The flexibility of the proteins was first quantified by the root mean square fluctuations (RMSF) of the C_α atoms (Figures 2 and S3). Among the three proteins, hGBP1$_{\mathrm{apo}}$ is the most flexible with RMSF values of up to 15.8 Å in the M/E domain, followed by mGBP2 with maximal RMSF values of 5.1 Å at residue 481—which is the tip of the M/E domain—in the apo-state and 6.4 Å at residue 422 of α10 in the GTP-bound state, while mGBP7 is the least flexible with maximal RMSF values at residue 588 of α13, reaching 4.1 Å in mGBP7$_{\mathrm{apo}}$ and 4.9 Å in mGBP7$_{\mathrm{GTP}}$. The different protein flexibilities are also visible in Figure 2 where the protein structures are colored according to the RMSF values.

2.2.2 | G domain motions

In mGBP2, binding of GTP stabilizes the G motifs and loops of the G domain, especially also the guanine cap, which is not so much the case for mGBP7. Except for the P-L motif, these motifs and loops in mGBP7$_{\mathrm{GTP}}$ remain flexible with RMSF values above 2 Å (Figures 2 and S3). To further characterize the motions of the G domain motifs and loops, we performed a clustering analysis of

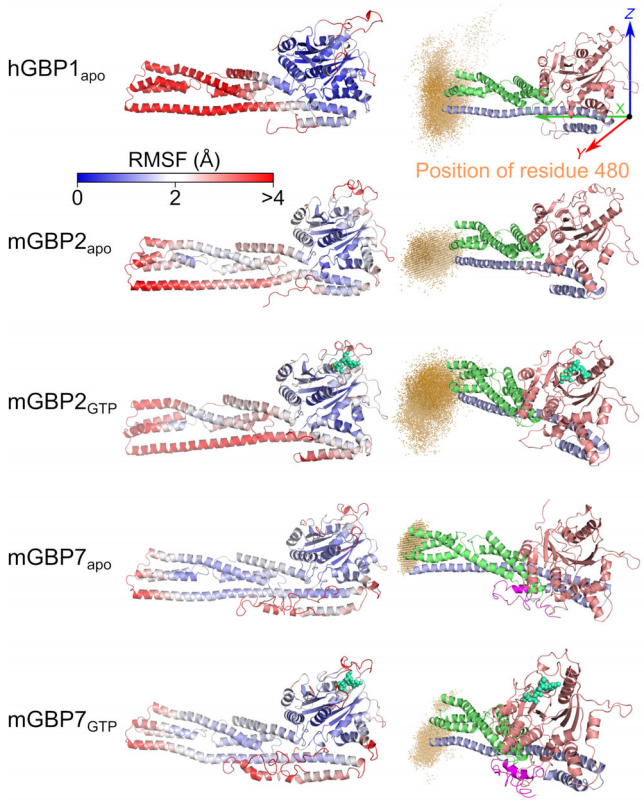

FIGURE 2 Structural fluctuations of the monomeric human GBP1 (hGBP1), murine GBP2 and 7 (mGBP2 and mGBP7). (Left) The protein flexibility, as quantified by the root mean square fluctuations of the C_α atoms during the respective HREMD simulation, is projected onto the initial structure of $hGBP1_{apo}$, $mGBP2_{apo}$, $mGBP2_{GTP}$, $mGBP7_{apo}$, and $mGBP7_{GTP}$. Rigid residues are colored in blue ($\lesssim 1.5$ Å) and flexible residues are shown in red ($\gtrsim 2.5$ Å), according to the color scale at the top. (Right) The spatial distribution of the residue 480 (i.e., the tip of the M/E domain) is shown as orange cloud to illustrate the hinge movement of the corresponding guanylate-binding protein monomer. Taking $hGBP1_{apo}$ as an example, the definition of the coordinate system is shown for the quantification of the hinge movement using the motions of the residue 480 with respect to the initial structure, denoted as d_{480}.

the G domains, with the simulation snapshots being fitted onto the β-sheets of the G domain. The resulting numbers of clusters, their populations, and maximal structural differences between the clusters are summarized in Table S2. The cluster data show that among the apo-states, mGBP2 has the most stable G domain, which becomes even stiffer in $mGBP2_{GTP}$. In mGBP7, the G motifs and loops are generally more flexible than in mGBP2 and the stabilization by GTP binding is also smaller (Figure S4). This is most significant for the guanine cap, for which the number of clusters decreases only by 14% from $mGBP7_{apo}$ to $mGBP7_{GTP}$ as compared to a 90% reduction in mGBP2. The different dynamics of mGBP7 motifs and loops compared to hGBP1 and mGBP2 largely correlate with the altered amino acid composition. In particular, the negative charge of the guanine cap in mGBP7, in contrast to the charge neutrality of this region in the other two proteins, is likely the cause of the generally higher flexibility and electrostatic repulsion of GTP. This further prevents its stabilization in $mGBP7_{GTP}$ as seen in $mGBP2_{GTP}$ where the guanine cap becomes more ordered (Figure S4). Interestingly, the relatively high flexibility of the G domain of mGBP7 does not affect the binding affinity of GTP, which is even higher for mGBP7 than for hGBP1 and mGBP2 (Table S1). It thus seems to be sufficient if the amino acid residues directly involved in GTP binding, such as R48 and K51 become rigid if GTP is present in order to enable a stable GTP binding site.

2.2.3 | Hinge movement of the M/E domain

The dynamics of the M/E domain is characterized as a hinge movement, as first discovered for hGBP1 (Barz et al., 2019) and then confirmed for mGBP2 (Loschwitz et al., 2023). To quantify that motion, we computed the distance of residue 480 at the tip of the M/E domain relative to its start position in the crystal structure or homology model during the HREMD simulations (denoted as d_{480}, summarized in Table S3 for all systems). Furthermore, we displayed the movement of this residue by calculation of the spatial distribution function, which is shown as orange dots in Figure 2. In hGBP1, the motion of residue 480 is the highest of all three GBPs, with the d_{480} values reaching up to 69.8 Å. The maximum movement of residue 480 in mGBP2 is slightly lower, due to the greater helical stability of α12 in mGBP2 resulting from the greater number of intrahelical salt bridges (30 vs. 21), but can also reach values of about 60 Å ($mGBP2_{apo}$: max. $d_{480} = 62.4$ Å; $mGBP2_{GTP}$: max. $d_{480} = 58.9$ Å). In mGBP7, the hinge movement is considerably smaller ($mGBP7_{apo}$: max. $d_{480} = 35.2$ Å; $mGBP7_{GTP}$: max. $d_{480} = 37.5$ Å), which can be also seen from the spatial distribution of that residue (Figure 2). The smaller M/E domain motions in mGBP7 can be correlated to a higher helical stability of α12 due to a wider distribution of oppositely charged residues across this helix than in hGBP1 and mGBP7, and from stabilizing interactions of α12 with the neighboring CT tail.

2.2.4 | Salt bridges

We conclude the analysis of the MD simulations of the GBP monomers by evaluating the stability of selected salt

bridges. Here, the selection was based on two criteria: (i) salt bridges previously shown to be relevant for the dimerization of hGBP1, particularly within the guanine cap and between α4′ and α12/13 (Ince et al., 2020; Vöpel et al., 2010), and (ii) salt bridges that showed significant changes in the population after dimerization of the GBP of interest, as revealed by the comparison of the MD simulations of the GBP dimer (see below) and monomer. The selected salt bridges are shown in Figure 3a and their occurrences during the simulations are summarized in Figure 3b. In $hGBP1_{apo}$, the salt bridge between K63 and E256 or E257 in the guanine cap has an occurrence below 15%, while a very stable salt bridge with 98% probability formed between R227 of α4′ and E556 or E558 of α12. In the corresponding simulation of $mGBP2_{apo}$, the salt bridge in the guanine cap (R62–E253) was more stable, with a probability of 40%. However, upon GTP binding this probability decreased to 16%, which can be explained by the ordering of the guanine cap in $mGBP2_{GTP}$, allowing the residue R62 to also interact with E249 with 77% probability (only 1.7% in $mGBP2_{apo}$). The salt bridges K226–E573 and R231–E554 tethering α12/13 to α4′, are stable in both mGBP2 states with probabilities of over 70%, while the salt bridge R225–E561 does not exist in either monomer state. In mGBP7, the salt bridge R57–E254 in the guanine cap is stable independent of the GTP binding state, which agrees to the observation that also the structure of the mGBP7 guanine cap is hardly affected by GTP binding. The other possible salt bridge, R57–D255, is only formed in $mGBP7_{GTP}$, yet also only with 9% probability. With regard to the α4′–α12/13 interactions in mGBP7, there are several possibilities for salt bridges, in particular between E222 and R566/K567 as well as R225 and D558/E562. They were all stable in both $mGBP7_{apo}$ and $mGBP7_{GTP}$ with occupancies above 50%. The only exception is the E222–R566 salt bridge in $mGBP7_{apo}$ for which only a 13% occupancy was found. An interesting difference between mGBP7 and the other two GBPs is that α4′ of mGBP7 donates a positively and a negatively charged residue for the formation of salt

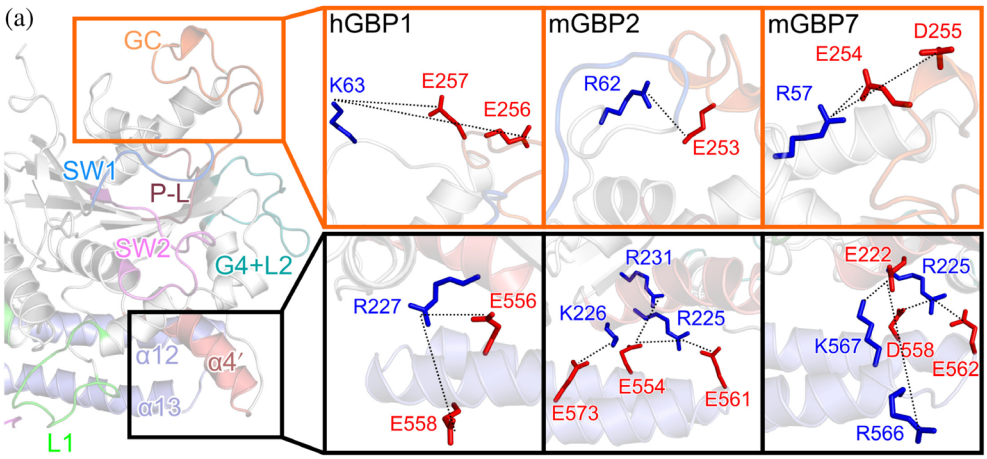

(b)

	hGBP1 (%)			
	K63–E256	K63–E257	R227–E556	R227–E558
$Monomer_{apo}$	13	9	98	0
Dimer	0/0	0/1	82/0	22/0

	mGBP2 (%)				
	R62–E253	R225–E554	R225–E561	K226–E573	R231–E554
$Monomer_{apo}$	40	95	0	84	70
$Monomer_{GTP}$	16	86	0	72	77
Dimer	27/55	84/100	79/28	53/46	0/0

	mGBP7 (%)					
	R57–E254	R57–D255	E222–R566	E222–K567	R225–D558	R225–E562
$Monomer_{apo}$	40	0	13	56	91	80
$Monomer_{GTP}$	41	9	75	54	77	97
SAXS model 1	59/37	0/0	84/0	56/48	95/76	85/28
SAXS model 2	71/22	0/0	0/74	83/74	34/67	85/90
Dimer model 1	99/66	67/22	2/98	82/14	72/82	0/0
Dimer model 2	72/95	0/46	1/71	73/48	68/95	0/3
Dimer model 3	24/61	0/0	0/0	4/23	33/42	96/95

FIGURE 3 Intramolecular salt bridges relevant for dimerization. (a) On the left, parts of the G and the E domain are shown. The location of the salt bridges within the guanine cap and between α4′ and α12/13 are indicated by an orange and a black box, respectively. On the right, the zoomed views of these areas are shown for human GBP1 (hGBP1), murine GBP2 and 7 (mGBP2 and mGBP7). The possible salt bridges are indicated by dotted lines between the residues being involved, which are labeled and their side chains are highlighted as red and blue sticks for negatively and positively charged residues, respectively. (b) Occupancy (in %) of the salt bridges during the simulations. The results for chain 1 and chain 2 are given separately for the dimers. The results are colored based on the occupancy: 0%–49%, red; 50%–74%, yellow; 75%–100%, green. P-L, P-loop; SAXS, small-angle x-ray scattering.

bridges with α12/13, whereas in hGBP1 and mGBP2 only positively charged residues in α4′ are available for electrostatic interactions with α12/13. Apart from that, the overall conclusion is that in all three proteins there are stable salt bridges between the G and the E domain that kept the three helices α4′, α12, and α13 closely together independent of the GTP loading state.

2.2.5 | Summary

We clearly observed different protein dynamics in mGBP7 compared with mGBP2 and hGBP1. Interestingly, mGBP7 shows greater dynamics in the G domain independent of GTP loading, whereas its M/E domain is more rigid than in the other two GBPs. In contrast, the G domain of mGBP2 stabilizes upon GTP binding, whereas the M/E domain remains flexible. This behavior is very similar to that of hGBP1. The difference in protein dynamics can be explained by both amino acid sequence and salt bridges formed in the proteins.

2.3 | Dimer models of GBPs

We continue our study by providing possible structural models for the mGBP2 and mGBP7 dimers and assessing the stability and motions of these dimers using MD simulations. This also includes the hGBP1 dimer, which serves as a reference as structural data for this dimer are at least partially available in the PDB. We first present the results of SAXS for mGBP7 and then proceed to protein–protein docking for mGBP2 and mGBP7, in the latter case complemented by XL-MS data.

2.3.1 | Small-angle x-ray scattering of mGBP7

With SAXS we aimed to reveal the mGBP7 dimer organization. To do this, we used a protein concentration range of 1.66–6.85 mg/mL and merged the scattering vector (**s**) data from the different protein concentrations. All relevant SAXS data are summarized in Table S4 and the corresponding SAXS analyses are shown in Figure 4a–d. We first used GASBOR (Svergun et al., 2001) to generate the molecular envelope of the dimer from the SAXS data, assuming P2 symmetry. The resulting envelope can be seen in Figure 4e,f. It deviates from the scattering data with a χ^2 of 1.14 (Figure 4a). With the Guinier approximation (Guinier, 1939), we determined the radius of gyration (R_g) as 5.35 nm for that envelope and used the distance distribution, shown as the *P*(distance) function, to specify the maximum particle dimension (D_{max}) as 17.0 nm (Figure 4b,c). The dimensionless Kratky plot (Figure 4d) as well as the *P*(distance) function showed a compact but elongated shape for the mGBP7 dimer. To obtain a structural model for the mGBP7 dimer, we fit two mGBP7 molecules into the GASBOR-generated envelope. The resulting model (Figure 4e), referred to as the SAXS model 1, has a protein–protein interface between the E domains and has a R_g of 5.03 nm and a D_{max} of 17.3 nm (see Table S5 for a summary of these values). By backcalculating the theoretical intensity with CRYSOL (Svergun et al., 1995) for the SAXS model 1 and comparing it with the experimental scattering data, this results in a χ^2 of 1.89. As this value is somewhat large, we created a further dimer model (denoted as SAXS model 2) using SASREF (Petoukhov & Svergun, 2005), which performs quaternary structure modeling of a complex formed by subunits with known atomic structure against the SAXS data set. The resulting model has larger R_g and D_{max} values compared to SAXS model 1 (5.67 and 19.1 nm, respectively), yet the χ^2 is closer to 1 with a value of 1.27 (Table S5). Like SAXS model 1, this dimer has a tail–tail interface, yet the dimerization is predicted to occur via the M domains (Figure 4f).

To test the stability of these two SAXS models, we simulated them for 100 ns. However, both dimers turned out to be unstable, as revealed by the RMSF and principal component analysis (PCA) to identify the most prominent collective motions (Figure 4g,h). Both dimers are very flexible as supported by the RMSF analysis, which was calculated after aligning the whole dimer. While the initial protein–protein interfaces with 2224 and 1560 Å^2, respectively, were considerably large at the beginning (Table S3), they notably decreased during the MD simulations. SAXS model 1 lost one of the two main interprotein contact interfaces, and the PCA revealed that the two proteins moved away from each other. This can be explained by the accumulation of negative charges at the original dimer interface, as shown by the EPS in Figure 4g. Similar observations were made for the SAXS model 2, where the initially symmetric interaction via the top parts of the two M/E domains broke within the 100 ns MD simulation and was replaced by an asymmetrical stalk tip–G domain interaction (Figure 4h). As for SAXS model 1, a considerable accumulation of negative charges at the original dimer interface is the reason for the instability of this dimer model.

2.3.2 | Model generation via protein–protein docking

Next, we applied protein–protein docking to generate possible mGBP7 dimer structures and compared them

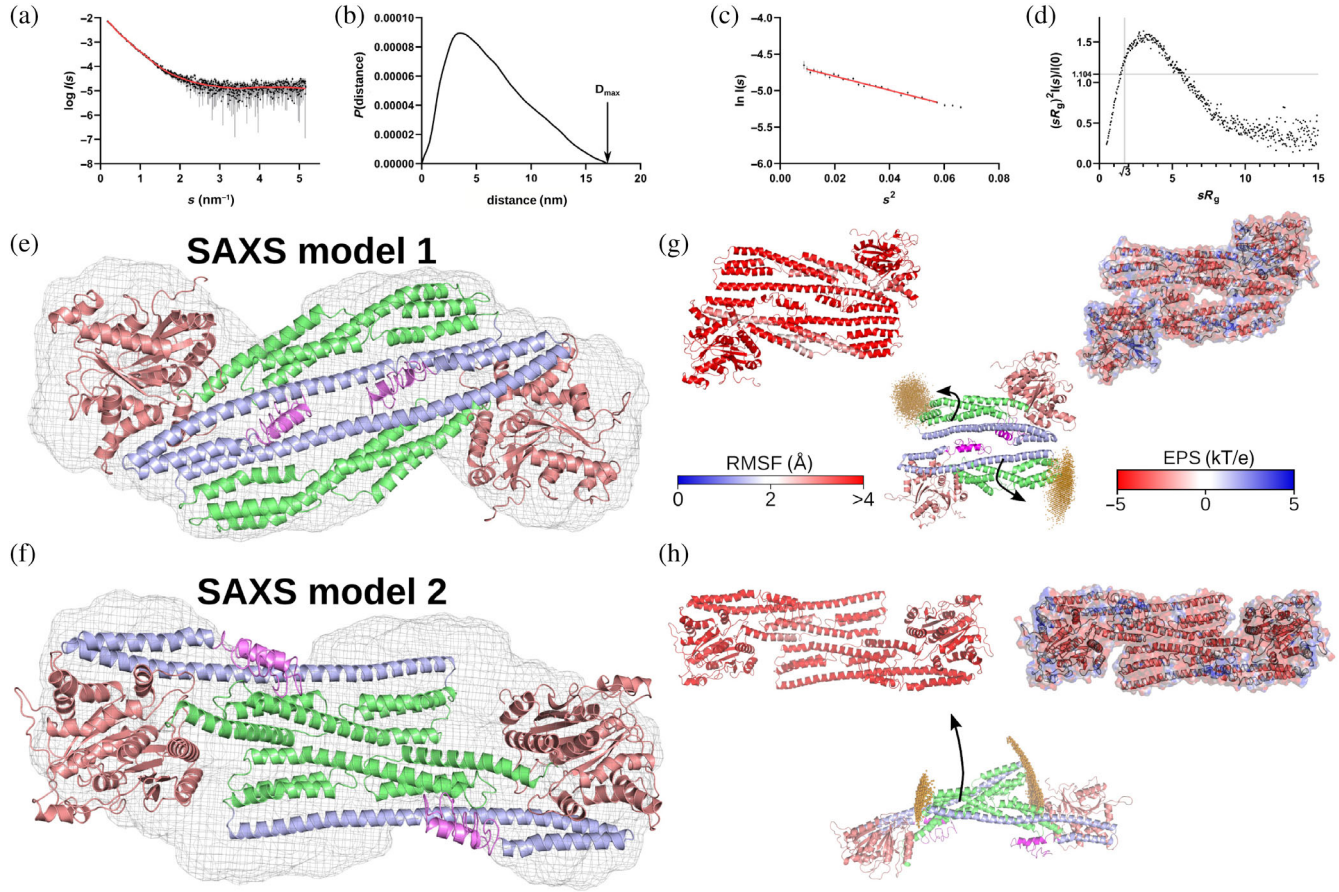

FIGURE 4 Murine GBP7 (mGBP7) dimer models from small-angle x-ray scattering (SAXS) data. (a) SAXS scattering data showing the intensity as a function of momentum transfer *s*. The experimental data is given as black dots with gray error bars, and the red line is for the GASBOR ab initio model fit (χ^2 of 1.14). (b) The distance distribution, shown as the *P*(distance) function, yields a maximum particle diameter (D_{max}) of 17.0 nm. (e) The Guinier plot reveals a Guinier region (red line) in the range of $sR_g < 1.3$, leading to a R_g of 5.35 nm. (f) The Kratky plot agrees with a compact elongated shape with certain flexibility for the mGBP7 dimer. (e) The SAXS envelope calculated with GASBOR and an mGBP7 dimer fit into it (SAXS model 1) are shown. (f) The same envelope but with the dimer model created with SASREF (SAXS model 2) is shown. (g) and (h) The stability of SAXS models 1 and 2 was tested in molecular dynamics simulations that were analyzed by the root mean square fluctuations (RMSF; left; red for flexible residues with RMSF $\gtrsim$ 2.5 Å), the electrostatic potential surface (right; red: negatively charged, white: uncharged, blue: positively charged), a principal component analysis with the main motions indicated by arrows (bottom), and the measurement of the hinge movements, which are shown as the spatial distribution of residues 480 in the proteins composing the dimer (orange clouds in the respective bottom plots).

with the SAXS and XL-MS data to identify those consistent with the experimental data. Because structural data are not yet available for the mGBP2 dimer, we also applied protein–protein docking to this protein, whereas for hGBP1 we used the dimer structure that exists for its G domain. To be precise, we created the hGBP1 dimer model by aligning the G domains of two hGBP1 monomers using the crystal structure of PDB ID 1DG3 (Prakash et al., 2000) to the dimer structure formed by two G domains (PDB IDs: 2B8W, 2B92, and 2BC9; Ghosh et al., 2006). The resulting dimer structure is shown in Figure 5a. It should be noted that we modeled the hGBP1 and mGBP2 dimers with GTP being bound as both proteins only notably dimerize in the presence of GTP (Ghosh et al., 2006; Kravets et al., 2012; Prakash et al., 2000), whereas mGBP7 was considered in its apo-state as the dimerization of this protein is not affected by GTP (Legewie et al., 2019) and the experimental mGBP7 data obtained here was also recorded without GTP.

Because proteins from the dynamin superfamily are known to adopt different dimer structures (Bian et al., 2011; Byrnes & Sondermann, 2011) (see also Figure 1e), we tested for the existence of alternative hGBP1 dimerization motifs using ClusPro (Kozakov et al., 2017), which is a physics-based protein–protein docking program. As such, it does not incorporate structural information from the PDB (Berman et al., 2000). However, the hGBP1 dimer structure with the highest

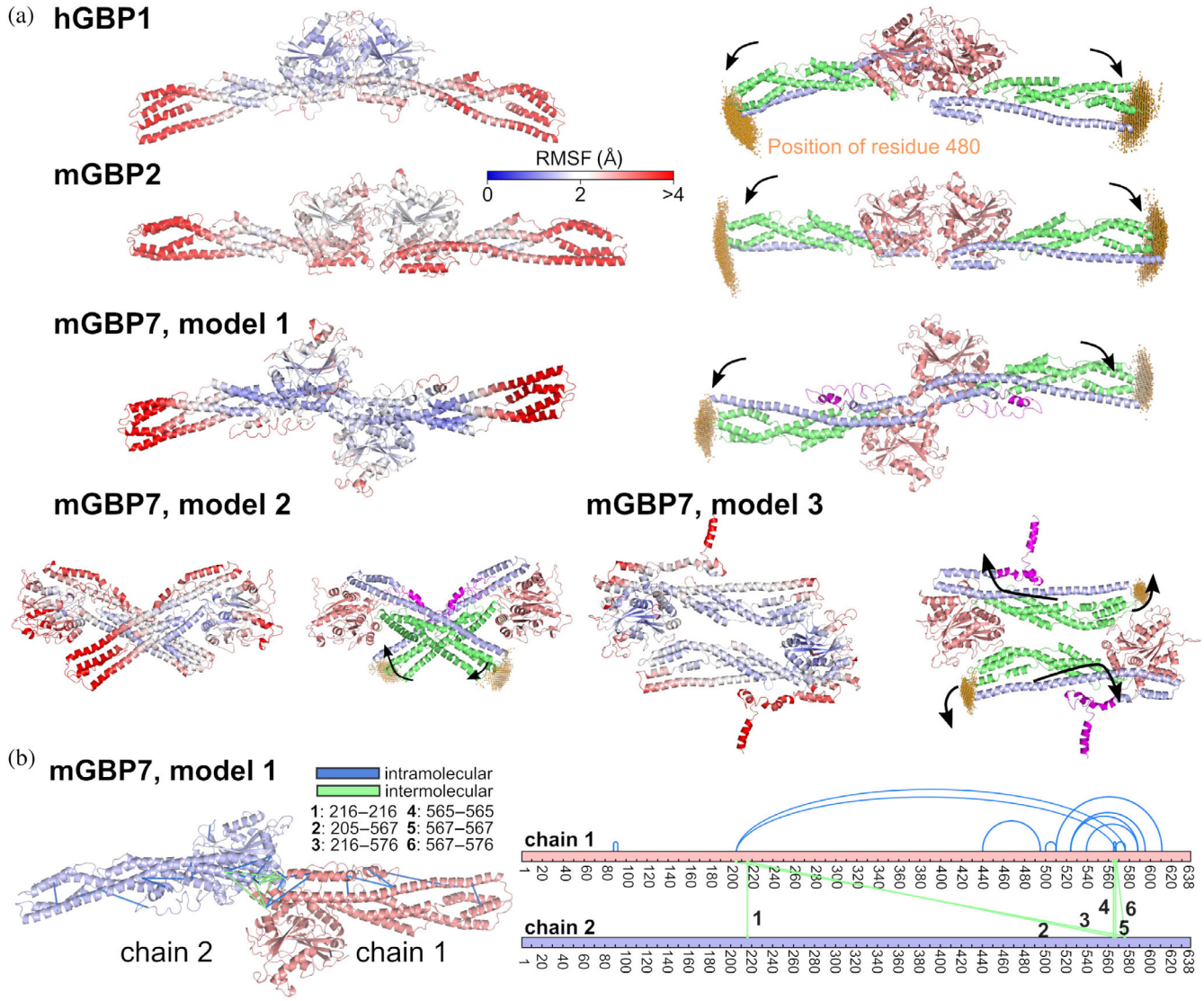

FIGURE 5 Dimer models for human GBP1 (hGBP1), murine GBP2 and 7 (mGBP2 and mGBP7) and their structural properties and comparison with crosslinking mass spectrometry data. (a) The overall stability of the dimers was quantified by the root mean square fluctuations (RMSF) of the C_α atoms during the molecular dynamics simulations of these dimers (left plot per dimer model). The RMSF was calculated by aligning the whole dimer and is projected onto the initial dimer model, where rigid residues are colored in blue and flexible residues in red (color scale at the top). The degree of the hinge movement of the M/E domains was determined by the spatial distributions of the residue 480, which are shown as orange clouds (right plot per dimer model). The coordinates used for measuring the hinge movement are the same as in Figure 2, with each chain of the dimers being aligned individually in that coordinate system. The black arrows indicate the main motions resulting from the principal component analysis. (b) Visualization of the crosslinks matching model 1 for the mGBP7 dimer. Mapped intermolecular crosslinks (numbers of the linked residues are given) are shown in green, while intramolecular crosslinks are colored in blue. Crosslinks are indicated in the 3D model (left) and in a linear sequence plot (right; created with xiNET; Combe et al., 2015).

docking score proposed by ClusPro is very similar to the hGBP1 dimer created from the structure of the G domain dimer. Their RMSD from each other is only 5.0 Å, which is small for the system size under consideration, and their topological similarity based on the so-called transmembrane (TM)-score calculated with MMalign (Mukherjee & Zhang, 2009) is rather high with a value of 0.73. The TM-score can range between 0 and 1, with 1 corresponding to a perfect match between two structures, and a TM-score of >0.5 indicating that two structures have a similar topology. The ClusPro docking scores for the other hGBP1 dimer models were low, and we therefore did not consider them in our further studies.

A similar picture emerged from protein–protein docking applied to mGBP2, which is understandable when considering its 76.3% sequence similarity with hGBP1. The most likely mode of dimerization predicted by ClusPro is via the G domains, leading to an mGBP2 dimer

model that is very similar to the crystal structure-based model for hGBP1 (Figure 5a). The following five best mGBP2 dimer models are also all G domain dimers, suggesting that this interaction interface is quite robust. The application of AlphaFold-Multimer (Evans et al., 2021) produced the same outcome, that is, only G domain dimers were suggested for mGBP2 (Loschwitz et al., 2023). Therefore, only the top mGBP2 dimer model produced by ClusPro was considered here.

For mGBP7, the situation is different. Here, ClusPro generates three different dimerization modes with top scores of equal probability (Figure 5a, hereafter referred to as models 1–3). None of these mGBP7 dimers involves the G domain interface seen for hGBP1 and predicted for mGBP2. ClusPro did not produce such a dimer model. Interestingly, the application of AlphaFold-Multimer (Evans et al., 2021) to mGBP7 creates only G domain dimers (Figure S5), yet their DockQ scores are low with respect to mGBP2 as reference. They are between 0.3 and 0.4, while only values between 0.8 and 1 (the possible maximum) indicate a similar protein–protein interface (Basu & Wallner, 2016). This poor match between mGBP2 and mGBP7 can be rationalized with the different amino acid compositions of their guanine caps. Instead, mGBP7 shows a strong tendency to dimerize via its stalks in an antiparallel arrangement. This is seen for models 2 and 3 created by ClusPro, and also applies to the next five best docking predictions, which are not further discussed here. The crossed-stalks motif present in model 2 is reminiscent of the dimerization pattern observed for other members of the dynamin superfamily (Noel et al., 2019; Reubold et al., 2015). Only the dimerization mode of model 1 involves the G domains, but also parts of α12/13, which is different from the G domain dimers observed for hGBP1 and mGBP2.

To assess the stability and dynamics of the hGBP1, mGBP2, and mGBP7 dimers shown in Figure 5a, we performed 100 ns MD simulations per dimer and calculated the RMSF and stalk-tip motions. Moreover, a PCA was applied to the MD data to identify the most prominent collective motions. To assess the dimer interface, we calculated the dimer contact area, analyzed selected salt bridges (see Figure 3), and determined the energies of the intermolecular contacts.

2.3.3 | Structural details of the hGBP1 and mGBP2 dimers

The dimerization via the G domains of hGBP1 and mGBP2 allows to bury a large protein area (Table S3). Of all dimer models discussed here, the hGBP1 dimer has the largest interface, with 5314 Å^2, and also the mGBP2 dimer model is stabilized by a large interaction area of 3129 Å^2. To assess the overall stability of the dimer, we calculated the RMSF after alignment of the whole dimer (Figure 5a), which shows that the hGBP1 dimer is stiffer than the mGBP2 dimer. The flexibilities of the chains within the dimers (Figure S6), calculated after separate alignment of each chain, are very similar to the RMSF profiles of the corresponding monomers, suggesting that dimerization does not have a large effect on protein movements. As for the monomers, the stalk tips are the most flexible, with RMSF values of up to 8 Å. Notably, in the monomer state, mGBP2 is less flexible than hGBP1, while it is the other way round in the dimers. Other flexible regions in both dimers are L1, G4 + L2, α4′, and the guanine cap. Nonetheless, compared to the monomers, the guanine cap as well as SW1 are stabilized, which correlates with salt bridge formation between the two chains (Figure 3a). The two hinge movements per dimer, measured as d_{480} (Table S3) and illustrated by the spatial distribution of residue 480 in Figure 5, are more pronounced in mGBP2. In either dimer, these hinge movements are correlated with each other, as revealed by the PCA. The first principal motion can be likened to a butterfly motion (see arrows in Figure 5a), leading to dimer geometries that are more curved or C-shaped, which is accompanied by the formation of an intramolecular contact between residues K62 and D255 (Figure 3b) and unfurling of the C-terminal regions (yet more so in one of the two chains per dimer).

The structure of the guanine cap is stabilized in both dimers compared to the monomeric proteins, yet the stabilization originates from partly different interactions in the hGBP1 and mGBP2 dimer (Figure 3). The occurrence of the intramolecular salt bridge K63–E256/E257, which already in the monomer only occurred with a probability of ∼10%, is abolished in the hGBP1 dimer. The corresponding salt bridge R62–E253 in the mGBP2 dimer gained in strength with respect to the mGBP2$_{GTP}$ monomer, reaching a chain-averaged occurrence similar to the 40% observed for the mGBP2$_{apo}$ monomer. The α4′–α12/13 lock is overall weakened in both dimers, but more so in the hGBP1 dimer. In mGBP2, where more salt bridges between α4′ and α12/13 are possible, the R225–E554 interaction is of particular stability and remains intact with a >84% probability in all mGBP2 systems studied here. With regard to intermolecular interactions (Figure S7), the hGBP1 dimer harbors strong (about −80 kJ/mol) contacts involving both guanine caps, such as E261–K252′, K252–D239′, and R245–E251′/E256′, as well as E105–K209′ (where the prime indicates that these residues belong to the other chain), which are mostly Coulombic in nature. The mGBP2 dimer is also held together by interactions between both guanine caps, but

further involves interactions of residues in the 130ies and of the G4 + L2 motif that form contacts with their respective counterpart in the other chain. The single strongest interaction is that of D237–R238′, with an interaction energy of −120 kJ/mol.

2.3.4 | Structural details of the mGBP7 dimers

Comparison of the models to experimental data

The three mGBP7 dimer models produced by docking (Figure 5a) were compared to the XL-MS and SAXS data obtained within this study. For the XL-MS experiments, recombinant mGBP7 was incubated in solution with either of two crosslinkers: bis(sulfosuccinimidyl) suberate (BS3, spacer arm length of 11.4 Å) or disuccinimidyl sulfoxide (DSSO, spacer arm length of 10.1 Å). Both crosslinkers react mainly with lysine residues and can link two lysines within a distance of 12 Å. The resulting mGBP7 dimers were separated from the monomers in a polyacrylamide gel and then analyzed by mass spectrometry. Crosslinked peptide pairs were subsequently mapped to the different mGBP7 dimer models created with ClusPro and to the mGBP7 monomer, as summarized in Table S6. A focus of the analysis was the identification of potential intermolecular contact sites within the homodimer, for which especially bridges between the same residues (like 216–216′, 565–565′, 567–567′)—as revealed by BS3 crosslinking—were informative. Of the three mGBP7 dimer models that resulted from docking, only model 1, which has an elongated shape with the dimer interface being formed via the G domain edges and the neighboring ends of α12/13, agrees with our crosslink information (Figure 5b). We also tested if the G domain dimers predicted by AlphaFold-Multimer (Figure S5) matched the XL-MS data, but they did not. The XL-MS intermolecular contacts can be mapped to the α4′ of the G domain and α13 of the E domain. Moreover, the interactions 205–567′, 216–576′, and 567–576′ for BS3 as well as 106–216′, 205–554′, 205–565′, and 557–567′ for DSSO are in agreement with the intermolecular contacts in this model. In conclusion, model 1 is the most probable model that fits to the XL-MS results. It fulfills three of the four constraints imposed by XL-MS. Regarding the fourth constraint, it should be noted that it clashes with the other three constraints, as revealed by a DisVis analysis using the HADDOCK web server (van Zundert & Bonvin, 2015), indicating that no single dimer model would be able to fulfill all four XL-MS constraints at the same time. This indicates a transient conformational change or that more than one dimer shape can be assumed.

We further tested how good models 1–3 are in agreement with the SAXS data. To this end, we docked them into the calculated molecular envelope and calculated theoretical SAXS data with CRYSOL. Table S5 lists the resulting χ^2, R_g, and D_{max} values. While a χ^2 close to 1 is desirable, also large deviations from the experimentally determined values of $R_g = 5.35$ nm and $D_{max} = 17.0$ nm render a dimer model as disagreeing with the SAXS data. However, even more emphasis is given on the agreement for the physical dimensions R_g and D_{max} than on χ^2. Based on these considerations, model 3 created by ClusPro can be considered a suitable model. In fact, it is not so different from the SAXS model 2 (Figure 4), except that the two proteins are less shifted with respect to each other to avoid the accumulation of negative charge that occurred at the contact site between the two M domains in the SAXS model 2. Model 1 is the least likely to fit the SAXS data, as its total length is significantly greater than the SAXS envelope. A head-to-head interface via the G domains as predicted by AlphaFold-Multimer (Figure S5) is for the same reason also unlikely as its D_{max} value is in conflict with the calculated P(distance) function.

Structural fluctuations in the mGBP7 dimers

With regard to the dimer interface, model 3 buries the largest protein surface with 3414 Å^2, followed by model 1 (2678 Å^2) and model 2 (2581 Å^2). Model 2 even increased its dimer contact area during the MD simulation, indicating stability and optimization of this dimer structure. All three dimer models were stable in the MD simulations (Figure 5a) and are now discussed in more detail.

The flexibilities of the M/E domains of mGBP7 in the dimer model 1 differ from the structural fluctuations (measured by the RMSF) of the mGBP7 monomer and are more similar to those of the mGBP2 dimer (Figure S6). In particular α10 and α12 are more flexible in the dimer. The guanine cap is stabilized, involving stronger intramolecular salt bridges between R57 and E254/D255 than in the mGBP7$_{apo/GTP}$ monomers (Figure 3). Within both chains, α4′ and α12 remain connected via a network of four redundant salt bridges of which in either chain two remain highly occupied. The first principal component of dimer model 1 is a butterfly motion, wherein the hinges move in a correlated fashion to form a more curved dimer, while the CT tail unfurls from its pocket. The strongest intermolecular interactions in the mGBP7 dimer model 1 are between the L1 and α4′ (E161–K213′, S211–D164′), between α4′ and the E domain (G209–K567′, R222–R566′), and between the two E domains (R566–E562′) with interaction energies in the range of −80 to −40 kJ/mol (Figure S7). These are partly

the same residues as those involved in intramolecular salt bridges, showing the competition between intra- and intermolecular salt bridges, and explaining that the intramolecular salt bridge R225–E562 completely disappeared while those involving R566 or K567 were absent in one of either chain of the dimer.

The protein motions within model 2 are very similar to those in model 1, even though the dimerization interface is completely different. The intramolecular salt bridges in the guanine cap strengthened in both dimers compared to the monomer, while the number of salt bridges formed between α4′ and α12 is smaller, but the overall contact remains intact. The butterfly motion resulting from the synchronous hinge movements of both chains is also present in model 2. Nonetheless, the first principal motion is decidedly asymmetric, with the stalks twisting around each other, which results in a contact between one G domain to the stalk tip of the other chain. This can be correlated with the observation of dissolved salt bridges between α4′ and α12 and a higher stalk tip flexibility. The strongest intermolecular interactions are found for the two electrostatic interactions E389–K508′ and E399–R396′ reaching about −110 kJ/mol, with supporting weaker interactions around residues 510 and 610.

In model 3, the mGBP7 proteins are less mobile compared with the other dimer models and also the protein monomer (Figure S6). Only the CT tail remains flexible. The occupancy of the intramolecular salt bridge in the guanine cap is similar as in the mGBP7 monomer, and thus smaller than in the other dimers. Moreover, also three of the four salt bridges tackering α4′ and α12 together have an occupation below 50%, indicating an increased tendency of the E domain to detach from the G domain. However, the fourth salt bridge, R225–E562, remains present to a similar degree as in the monomer, whereas in models 1 and 2 this particular salt bridge was absent (Figure 3b). The first principal motion of model 3 results in a saddle-like structure where the rather planar shape of the dimer becomes more curved due to both stalk tips moving in the same direction. The tip of one of the M/E domains even detaches from the G domain of the other chain, enabling a larger range of motions for the E domains that together almost form a cross shape. The intermolecular interactions that contribute the most to the dimer stability are R33–D411′ and K26–E419′, reaching −120 and −60 kJ/mol, respectively, which are supported by weaker interactions between the guanine cap and the stalk tip (Figure S7). Moreover, the N-terminal E8 is also of relevance as it interacts with several residues of α10 of the other chain, summing up to an additional −140 kJ/mol of interaction energy.

3 | DISCUSSION AND CONCLUSION

We compared the sequence and biochemical properties of three GBPs, the human GBP1 and the murine GBP2 and GBP7. The main conclusion from that juxtaposition is that mGBP2 is more similar to hGBP1 than to mGBP7. Both hGBP1 and mGBP2 are posttranslationally modified by isoprenylation where instead mGBP7 exhibits 49 additional C-terminal residues for membrane binding. Moreover, the sequence of mGBP7 differs markedly at various places from those of hGBP1 and mGBP2. The different distribution of charged residues gives rise to different protein dynamics, as we revealed by HREMD simulations of the monomeric proteins. We generated dimer models for the three GBPs (Figure 6a). For hGBP1 and mGBP2, only dimerization via the G domains was identified, leading to the dimer also known as the head-to-head dimer, which in the case of hGBP1 contains the crystal structure of the dimer formed only by the G domains (Ghosh et al., 2006). For mGBP7, we obtained three dimer models, of which one model agrees with our XL-MS data (model 1), one contains a crossed-stalks motif also found for other members of the dynamin superfamily (Noel et al., 2019; Reubold et al., 2015) (model 2), and one is in fair agreement with our SAXS data (model 3). The latter model resembles one of the two mGBP7 dimer models that we created by directly fitting mGBP7 to the SAXS envelope. However, these two SAXS models were found to be unstable in the subsequent MD simulations because the physicochemical properties of the proteins were not taken into account during this fitting process. All dimer models shown in Figure 6a were stable in the MD simulations and are discussed below in light of the existing literature.

3.1 | General comparison of the dimer models

In order to understand the dimer dynamics, we first simulated the monomers of the three GBPs in solution serving as a reference. For mGBP2 and mGBP7, both the apo- and GTP-bound state were considered, while the hGBP1 monomer was only simulated as apo-protein. In the apo-state of the GBP monomers, the different motifs and loops of the G domains are very flexible, one reason being that R48, which serves as arginine finger, has no stable contact without GTP. The simulations further revealed that all three GBPs feature the characteristic hinge movement involving the M/E domain that we had originally uncovered for hGBP1 (Barz et al., 2019).

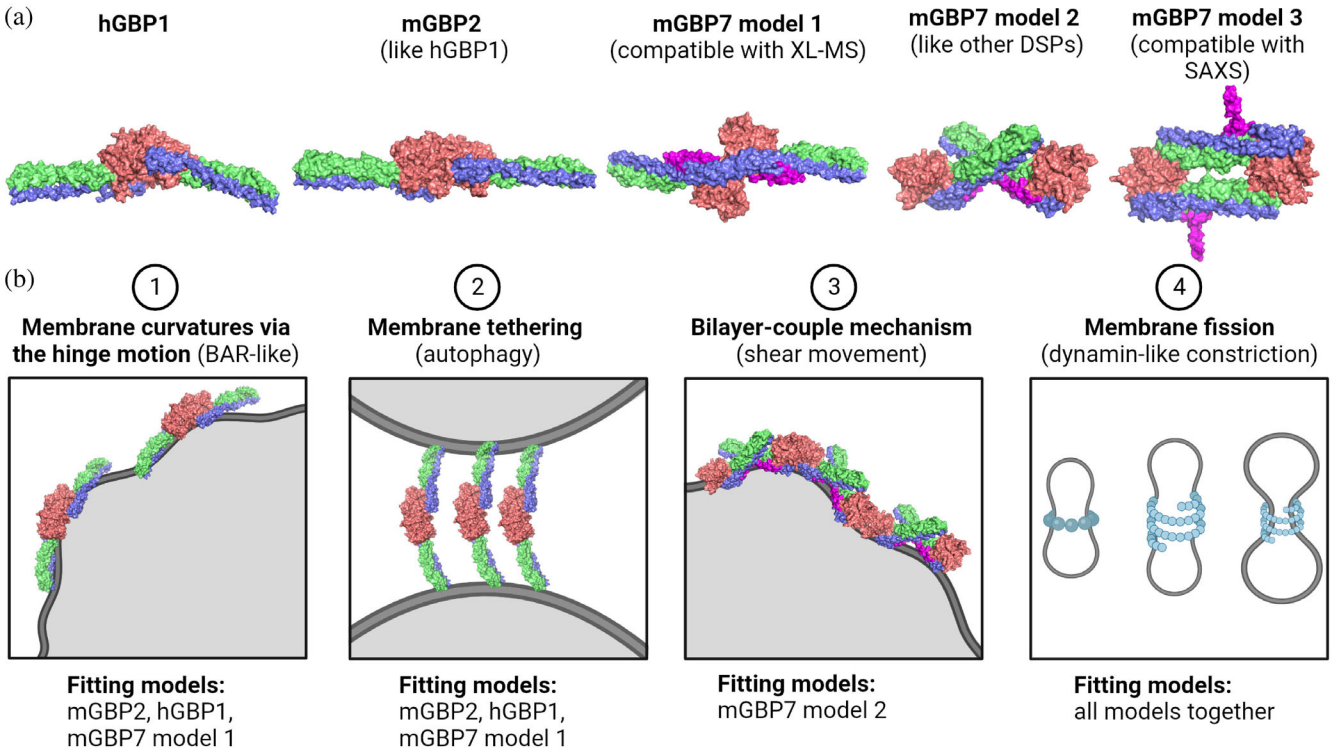

FIGURE 6 Summary of dimer structures and possible biological functions. (a) The dimer models of human GBP1 (hGBP1), murine GBP2 and 7 (mGBP2 and mGBP7) studied in this work are shown. (b) Different dimerization modes suggest various mechanisms of action: (1) A curving of the dimer could induce membrane curvature by the scaffold mechanism, similar to Bin/Amphiphysin/Rvs (BAR) domain proteins or the cytoplasmic coat proteins for vesicle transport (COP) machinery. (2) The G domain dimer of hGBP1, mGBP2, or model 1 of mGBP7 could serve to tether the parasite-related membrane to the autophagosome. (3) Insertion of tilted helices, which would be possible with mGBP7 dimer models 2 and 3, would give rise to the so-called local spontaneous curvature mechanism or bilayer-couple mechanism (McMahon & Gallop, 2005), ruffling the membrane or generating shearing forces. (4) Finally, by combining several of these dimerization modes, even a dynamin-like constriction would be imaginable. This figure was created with BioRender. DSPs, dynamin superfamily proteins; SAXS, small-angle x-ray scattering; XL-MS, crosslinking mass spectrometry.

Among them, hGBP1 exhibits the largest hinge movement and mGBP7 the smallest one. A probable reason for this is that the CT tail has a stabilizing effect on the M/E domain of mGBP7. Another difference is that the G domain of mGBP7 does not stabilize so much upon GTP binding as in mGBP2, especially the guanine cap does not adopt a structured conformation and remains flexible as in the apo-state. There are differences in the sequence of the mGBP7 guanine cap compared to hGBP1 and mGBP2. In particular, this motif is negatively charged in mGBP7, which would explain that binding of the negatively charged GTP has no stabilizing effect on it. This in turn further unfolds why none of the three techniques used for determining the mGBP7 dimer structures, that is, XL-MS, SAXS, and protein–protein docking, predicted the dimerization to occur via the two guanine caps. It is either too dynamic to allow a stable mGBP7 dimer to be formed and/or the amino acid composition does not allow strong enough interactions between the two guanine caps to evolve. In hGBP1 and mGBP2, the stabilization of the guanine cap via GTP binding seems to be a prerequisite for dimer formation, either to reduce the entropy penalty for the dimerization or to have a well-defined interaction surface. As the guanine cap seems not to be involved in mGBP7 dimerization, this further explains why this protein can be a transient dimer in the cytosol without GTP (Legewie et al., 2019).

Common observations for the dimer models are that the intramolecular salt bridges locking α4′ and α12/13 never completely dissolved, due to a redundancy of up to four salt bridges of which at least one is always present with $\gtrsim 50\%$ occupancy. Only in one of the chains of the hGBP1 dimer, all salt bridges between α4′ and α12 completely dissolved, which on longer time scales could give rise to a folding out of the E domain, as was already observed for hGBP1 multimers (Lorenz et al., 2020; Sistemich et al., 2020, 2021). The G domain dimers (hGBP1, mGBP2, and model 1 for mGBP7) show an increase in the stability of the intramolecular salt bridge within the guanine cap, which coincides with a structural

stabilization of the guanine cap, while this salt bridge is not stabilized in the stalk dimers of mGBP7 (models 2 and 3). All dimers are stabilized by intermolecular salt bridges, with one or two of them being of particular strength with interaction energies even below −100 kJ/mol, which are supported by several surrounding weaker interactions.

3.2 | Linking structural and mutation data to the current dimer models

3.2.1 | Dimer interface size

According to Bahadur et al., a biologically relevant dimer interface should comprise at least 1000 Å^2 (Bahadur & Zacharias, 2008). All dimer models studied here fulfill this criterion. Negi et al. (Negi & Braun, 2007) analyzed more than 70 protein complexes with known 3D structures and revealed that dimer contacts are often mediated by "hot spot" residues, meaning that only very few amino acids significantly contribute toward the binding energy. This is also reflected in our GBP dimer models. The interaction area is largest for the head-to-head dimer of hGBP1, indicating that this might be the "strong initial interaction" around which the polymer lattice on a lipid membrane is built (Daumke & Praefcke, 2016). Previous dimers reported for DSPs (some of which may only be due to crystal-packing) include the hGBP1 dimer by Prakash et al. (Prakash et al., 2000), burying 2890 Å^2 of surface area for head-to-tail dimerization via G domain–α 10/12 interactions, and 2140 Å^2 for the head-to-head arrangement. In 2006, Ghosh et al. (Ghosh et al., 2006) described an hGBP1 dimer that has an even larger interface of 3900 Å^2 and includes residues that are conserved in hGBP isoforms and the G domain motifs. The interfaces buried by the dimers studied here are within or even beyond that range, with values between 5314 Å^2 (hGBP1) and 2581 Å^2 (mGBP7, model 2). These interfaces thus fulfill the necessary size requirement for a stable dimer. The largest interface sizes were observed for the G domain dimers, which were also identified as the most stable dimers, further confirming the existence of this GBP dimerization mode.

3.2.2 | Salt bridges at the dimer interface

According to Praefcke et al., the residues 48–52 of hGBP1 are necessary for dimerization, especially R48 for building tetramers. Further residues involved, yet to a lesser degree, are 72, 76, 99, 103,106, 109, and 112 (Praefcke et al., 2004). We now understand the relevance of these residues for dimerization due to their importance in GTP binding and subsequent stabilization of the G domain, in particular the guanine cap. Moreover, our simulations of mGBP2 also revealed direct engagement in dimerization for two of the residues in that region, namely for R48, which has a small, but noticeable dimerization energy contribution, and E102, which shows a prominent interaction to a number of residues. For hGBP1, it was demonstrated that the α6 helix plays a critical role in dimerization, especially the residues 289–308, as well as residues 103–108 (Abdullah et al., 2010). While the former region was not close enough to the dimer interface in any of the dimers studied here, we can confirm that the latter region has a high energetic contribution to dimer formation of both hGBP1 and mGBP2.

Vöpel et al. (Vöpel et al., 2010) observed that two positively charged residues of hGBP1, R227 and K228, located on α4′, as well as four glutamate residues, 556, 563, 568, and 575, located on α12/13, form intraprotein salt bridges and that loosening their interaction facilitates dimerization and tetramerization. This can either mean that (i) α4′ and/or α12/13 are part of the interface causing the intraportein salt bridges to break, (ii) that they need to be broken in order to reveal the interface, or (iii) that dimerization could cause these salt bridges to break via an allosteric effect if α4′ and α12/13 should not be directly involved in the dimerization. Here, we observed effect (i) in the mGBP7 dimer model 1, where the mentioned salt bridges loosened enabling both α4′ and α12 to contribute to dimer formation at interaction interface. In 2012, Wehner et al. (Wehner et al., 2012) suggested that residues 105, 186, 245, and 259 have only minor effects on the dimerization of hGBP1, while residues 240 and 244 (i.e., the guanine cap) were identified to be essential for it. Our results for the head-to-head dimer of hGBP1 revealed R48, E105, K209, D237, D239, R242, K243, R245, K247, E251, K252, E256, E259, and E261 as main players in the dimerization, underlining the importance of the guanine cap. These residues have further in common that they are all charged, and under that aspect, R243 and K244 appear interchangeable. It is interesting to note that all of these residues are conserved between hGBP1 and mGBP2, supporting the formation of a head-to-head dimer in mGBP2. In summary, we can confirm the importance of residues in the guanine cap (230–245) for dimerization of hGBP1 and mGBP2. The salt bridge 62–255 that enhances dimerization shows a slightly increased formation in the dimer. Moreover, energy analysis of interfacing residues revealed that intramolecular salt bridges are partly replaced by intermolecular interactions.

3.3 | Biological relevance of different dimer structures

In order to understand why different GBP dimer structures may be adopted, it is instructive to recall their conformational dynamics. Upon dimerization, the hinge movements of the two proteins forming the dimer give rise to an overall correlated motion. In the cases of the mGBP2 dimer and model 1 of mGBP7, the two chains do not show a greater individual range of motions than their monomeric counterparts, but the extended length of the two proteins moving in a concerted fashion could introduce more stress on a membrane than a single GBP protein is able to do, comparable to the observations made for Bin/Amphiphysin/Rvs (BAR) domain proteins (Daumke et al., 2014; McMahon & Gallop, 2005; Zimmerberg & Kozlov, 2006). In contrast to that, the motions of dimer model 2 of mGBP7 do not lead to an increased overall curvature, so that a possible mechanism of introducing membrane stress/shearing force would require both the CT tails and the stalk tips to be inserted into the membrane. The insertion of a single (angled or short) helix can result in a hydrophobic mismatch that facilitates membrane fission (Fattal & Ben-Shaul, 1993), comparable to a wedge driven into the lipid bilayer. The dimer model 3 of mGBP7 involves a more flexible stalk tip than in the monomeric mGBP7 form, but the protein–protein interaction along the length of the M/E domains constricts the overall dynamic effect.

While these three notable structures seem initially to be at odds with each other, several studies of other DSPs are in support of the existence of different DSP multimer arrangements based on up to four intermolecular interfaces (Chen et al., 2017; Daumke et al., 2014). In the case of OPA1, dimerization can be both nucleotide-dependent and -independent, involve multiple interfaces apart from the G domain, and lead to higher order oligomers (Yu et al., 2020). It is possible that the structures spatially complement each other to form a lattice, a multimer consisting of several different dimers. On the other hand, the dimers may also temporally complement each other during the GTPase cycle, with rearrangements triggered by nucleotide binding or hydrolysis. Moreover, some dimer structures may not be functional and only be present during the aggregated/storage phase.

If we translate the structural information that is available for DSP multimers to the GBPs studied here, we conclude that the GBP dimer models could be combined to form a long string of half-moon shapes, comparable to the BAR domain proteins (Figure 6b). The primary, most stable interaction would happen via the G domains, with the underside of the E domains as in mGBP7 model 2 forming the second interface. The alternating rise and fall of the proteins could induce local curvature of the membrane, especially when considering the hinge movement of the M/E domains. Adding a third model (mGBP7 model 3), the dimers could even be integrated into a helical-ring-model, reminiscent of other dynamins. While the first turn of the helix consists of G and E domain interactions, the remaining M domain would form the inter-rung contacts. A conformational change of the M/E domain would be needed to "unlock" the fourth interface, the crossed-stalks dimer. This further requires that the G domain interface is flexible enough that a tilting of the spherical G domains against each other is still stable. The docking results indicate that such nonstandard G domain interfaces are possible. Such a ratchet-like tightening of the dynamin collar has been previously suggested (Ford & Chappie, 2019).

Furthermore, with more than one interface, the dissolution of less stable interactions could be prevented by a lattice of surrounding interactions, and additional binding of the CT tails to the membrane. The small sequence variations between hGBP1, mGBP2, and mGBP7 seem indeed to be sufficient to tip the scale in favor of other dimer structures. It might thus be possible that some of the isoforms act as chain-starters (with maybe only one stable interface), some as continuous elongators, and some as chain-breakers (with no further interfaces), a scenario in which heterooligomers of seemingly redundant proteins would be necessary. For bacterial DSPs, this has already been proposed (Liu et al., 2018). We further know that mGBP2 and mGBP7 co-localize at the parasitophorous vacuole membrane and that mGBP2 attaches first, followed by mGBP7, and that mGBP7 deletion is more lethal than mGBP2 deletion (Steffens et al., 2020). Perhaps mGBP7's various polymerization options allow a larger carpet of GBPs to form, which can then more effectively remodel membranes, something that should be addressed by future studies.

3.4 | Conclusion

The observations from our current work transcend the conventional sequence–structure–function paradigm in proteins (Liberles et al., 2012). Firstly, despite noteworthy differences in sequence between mGBP7 and its counterparts mGBP2 and hGBP1, they share an identical structural framework. While their dynamics may initially appear indistinguishable, a closer examination reveals nuanced distinctions. Remarkably, the sequence and dynamics disparities between mGBP7 and mGBP2/hGBP1 are substantial enough to prompt divergent dimerization patterns in mGBP7, which are anticipated to confer distinct functional attributes compared to mGBP2. This suggestion is consistent with our previous in vivo findings

that the absence of mGBP7 in mice infected with *T. gondii* results in higher mortality than deletion of mGBP2 (Degrandi et al., 2013; Steffens et al., 2020).

4 | METHODS AND MATERIALS

All details about the experimental methods are provided in the Supporting information.

4.1 | MD simulations and docking

4.1.1 | General aspects of the MD simulations

The structures of hGBP1, mGBP2, mGBP7 were prepared for the simulations as previously described, which includes the parametrization of GTP and the geranylgeranyl group (Barz et al., 2019; Legewie et al., 2019; Loschwitz et al., 2023). The hGBP1 dimer was created using MMalign (https://zhanglab.ccmb.med.umich.edu/MM-align/; Mukherjee & Zhang, 2009). For all MD simulations, the Amber99SB*-ILDNP force field (Aliev et al., 2014; Best & Hummer, 2009; Lindorff-Larsen et al., 2010) was used for modeling the proteins, the TIP3P model was used for water (Jorgensen et al., 1983), and GROMACS 2016 (Abraham et al., 2015, 2017) was employed for running the simulations. The simulation temperature and pressure were 310 K (37°C) and 1 bar, respectively. In Table 1, all MD simulations included in this study (total simulation time of 36.7 μs) are listed.

4.1.2 | HREMD simulation of the mGBP7 monomer

In our previous study of mGBP7 (Legewie et al., 2019), we already obtained the structure of mGBP7 by using homology modeling and simulated it as $mGBP7_{GTP}$ for 100 ns. The most populated cluster structure of that simulation was used here as starting point for the HREMD simulations of $mGBP7_{apo}$ and $mGBP7_{GTP}$. The protein was always placed in a rectangle simulation box of $10 \times 10 \times 18$ nm^3 dimensions, ~56,000 water molecules were added, as well as 10 (apo) or 13 Na^+ (GTP) for the neutralization of the systems, resulting in a total number of ~178,000 atoms. A similar HREMD protocol as applied in our study of mGBP2 (Loschwitz et al., 2023) was used and is described in detail in the Supporting information.

4.1.3 | Protein–protein docking

To obtain GBP dimer structures, we performed protein–protein docking and employed ClusPro (https://cluspro.bu.

TABLE 1 Summary of simulations included in this work.[a]

Simulation	System	Size in atoms	Runs	Length	Cumulated time
HREMD[b]	$hGBP1_{apo}$	335,553	1 × 30	400 ns	12 μs
HREMD[c]	$mGBP2_{apo}$	131,493	1 × 16	200 ns	3.2 μs
HREMD[c]	$mGBP2_{GTP}$	129,116	1 × 16	200 ns	3.2 μs
HREMD	$mGBP7_{apo}$	178,800	1 × 30	400 ns	12 μs
HREMD	$mGBP7_{GTP}$	178,019	1 × 30	400 ns	12 μs
MD	hGBP1 dimer	556,008	1	100 ns	100 ns
MD	mGBP2 dimer	556,729	1	100 ns	100 ns
MD	mGBP7 dimer, model 1	538,254	1	100 ns	100 ns
MD	mGBP7 dimer, model 2	308,874	1	100 ns	100 ns
MD	mGBP7 dimer, model 3	308,763	1	100 ns	100 ns
MD	mGBP7 dimer, SAXS model 1	308,514	1	100 ns	100 ns
MD	mGBP7 dimer, SAXS model 2	308,763	1	100 ns	100 ns
Total simulation time					36.7 μs

Abbreviations: hGBP1, human GBP1; HREMD, Hamiltonian replica exchange molecular dynamics; MD, molecular dynamics; mGBP7, murine GBP7; SAXS, small-angle x-ray scattering.

[a]The simulations reported in this work were either performed in the supercomputer JURECA at the Jülich Supercomputing Centre (Krause & Thörnig, 2018), in SuperMUC-NG at the Leibniz-Rechenzentrum (LRZ) in Munich, or in HILBERT at Heinrich Heine University Düsseldorf.

[b]This trajectory originates from reference (Barz et al., 2019).

[c]This trajectory originates from reference (Loschwitz et al., 2023).

edu) (Kozakov et al., 2017) for this purpose, taking favorable assessments of this program into account (Porter et al., 2019; Torchala et al., 2013). The multimer docking mode of ClusPro was used, both in combination with SAXS data and/or crosslinking data, and without additional restraints. The inclusion of additional restraints did not result in new structures, only a reordering of the results happened. From the top 10 results of the different setups, the most promising candidates were selected for MD simulations.

4.1.4 | MD simulations of the GBP dimers

The dimers were simulated in boxes with sizes, depending on the structure, varying from 18.5×12.5 13.5 to $27.0 \times 15.5 \times 13.5$ nm^3, with water added for solvation and NaCl added for neutralization. A two-step equilibration was performed as described for the HREMD simulation, yet without an additional *NpT* equilibration. The hGBP1 and mGBP2 dimers were simulated with GTP being bound, using a 2 fs time step, while the GTP-free mGBP7 dimers were simulated using a 4 fs time step (in combination with virtual sites). In all simulations, positional restraints of 1,000 kJ/(mol nm^2) were applied to the stable β-sheets of the G domains, in order to inhibit overall rotation. Given the elongated shape of the GBPs, overall protein rotation would have required considerably larger simulation box sizes. The Parrinello–Rahman barostat and Nosé–Hoover thermostat were used. Each dimer structure was simulated for 100 ns, where frames were saved every 20 ps and analyzed. In order to assess the dimer–dimer interactions, another 100 ns MD trajectory was produced per dimer, where additional energy groups were added to the GROMACS index file. For this, the first 100 ns trajectory was analyzed, and all residues within 7.5 Å of the other chain were included. This allowed us to identify the most strongly interacting residues in the second trajectory, which were energetically analyzed in detail.

4.2 | Analysis of the MD simulations

To generate figures of the 3D protein structures, we applied PyMol (PyMol, 2015). If not stated otherwise, the analyses were performed using GROMACS 2016. For the analysis of the HREMD simulations, only the target replica was used.

4.2.1 | Sequence alignment

The alignment of the sequences of hGBP1, mGBP2, and mGBP7 was done with T-Coffee (Notredame et al., 2000) using the default settings as available at the European Bioinformatics Institute (EMBL-EBI) web server (Madeira et al., 2019) (https://www.ebi.ac.uk/services). The resulting sequence alignment was visualized using Jalview 2 (Waterhouse et al., 2009) where we colored the residues according to their residue type.

4.2.2 | Root mean square fluctuations

For quantifying the flexibility of the GBPs, we calculated the RMSF of the C_α atoms around their average positions for each residue. A residue with a value over 2 Å is considered as flexible. For visualization, the RMSF values were color-mapped and projected onto the corresponding start structure of the simulations using red colors for flexible regions (RMSF $\gtrsim 2.5$ Å) and blue colors for rigid parts (RMSF $\lesssim 1.5$ Å).

4.2.3 | Electrostatic potential surface

The Adaptive Poisson-Boltzmann Solver as available in the PyMol plugin APBS 2.1 was used for the calculation of the electrostatic potential (Baker et al., 2001). To generate the required input files (*.*pqr* and *.*pot*), the web server https://server.poissonboltzmann.org with default settings and with pH 7 for the pK_a calculation was employed (Jurrus et al., 2018). For visualization, the electrostatic potential was color-mapped between −5 (red) and +5 kT/e (blue) and projected onto the surface presentation of the proteins.

4.2.4 | Movements of residue 480

To quantify and characterize the hinge movement of the M/E domain, the motions of residue 480 were monitored relative to the start structure of the simulations. To this end, the distance of that residue (d_{480}) was determined using our own visual molecular dynamics, (Humphrey et al., 1996) script after fitting the trajectory frames to the G domain of the start structure. To illustrate the hinge movement, we computed the spatial distribution function of residue 480 using the *gmx spatial* tool of GROMACS.

4.2.5 | Principal component analysis

To extract the main motions of the proteins, the PCA as implemented in GROMACS was performed. The covariance matrix was created with *gmx covar*, and the first two eigenvectors, also called principal components or

principal motions (PC1 and PC2), were determined using *gmx anaeig*. The trajectory was fitted to the C_α atoms, and for the generation of conformations along eigenvectors 1 and 2, the backbone was selected.

4.2.6 | Salt bridge analysis

To determine the occupancies of selected salt bridges, the distances between the atoms involved were determined. Following atoms of charged residues were used for the calculations: Lys—NZ; Arg—NE, NH1, NH2; Asp—OD1, OD2; Glu—OE1, OE2. A salt bridge was assumed to be present if the distance in question was within 4.5 Å. Salt bridge occupancies were calculated as time-averaged probabilities.

4.2.7 | Clustering analysis

To characterize the flexibilities of the G domain, we performed clustering analyses for the G motifs and loops using the algorithm of Daura et al. (Daura et al., 1999) as implemented in GROMACS. The clustering was applied to all atoms of the desired structural element with a C_α-RMSD cutoff of 2.5 Å to identify cluster membership. Before the clustering, the trajectory was fitted onto the β-sheets in the G domain.

4.2.8 | Protein–protein interface size

The size of the protein–protein interfaces was calculated using the difference in the solvent-accessible surface areas (SASA):

$$\mathrm{SASA}_{\mathrm{interface}} = (\mathrm{SASA}_{\mathrm{chain\,1}} + \mathrm{SASA}_{\mathrm{chain\,2}}) - \mathrm{SASA}_{\mathrm{dimer}}$$

For the SASA calculation, the GROMACS tool *gmx sasa* was used, with a probe radius of 1.4 Å.

4.2.9 | Analysis of dimer interaction energies

The energy groups of interacting residues as determined in the 100 ns MD simulations of the GBP dimers were added to the GROMACS index files and a second 100 ns MD simulation per dimer was performed. The resulting residue–residue energies were presented as a matrix, and the most negative energies were further analyzed by decomposing them into Coulomb and Lennard-Jones short-ranged interaction energies as calculated by GROMACS.

4.2.10 | SAXS-related analysis

To compare the mGBP7 dimer models with the SAXS results, R_g and D_{max}, we calculated the time-averaged values using the GROMACS tools *gmx gyrate* and *gmx principal*, respectively. The resulting values are denoted as R_g^{MD} and D_{max}^{MD}. For better comparability with the values obtained from SAXS, we calculated the theoretical scattering intensity with CRYSOL (Svergun et al., 1995) for the dimer models predicted by docking and determined their R_g and D_{max} values.

AUTHOR CONTRIBUTIONS

Wibke Schumann performed and analyzed simulations for the GBP dimers and wrote this part of the manuscript. Jennifer Loschwitz performed and analyzed simulations for the GBP monomers and wrote this part of the manuscript. Gereon Poschmann performed and analyzed the XL-MS experiments and wrote the respective paragraphs. Jens Reiners and Sander H. J. Smits performed and analyzed the SAXS experiments and wrote the respective paragraphs. Larissa Legewie, Daniel Degrandi and Klaus Pfeffer provided protein material and wrote the respective methods part. Daniel Degrandi, Klaus Pfeffer, and Kai Stühler provided infrastructure, supervision, and advised writing the manuscript. Birgit Strodel conceived the research project and provided infrastructure and extensive supervision. All authors were involved in revising the manuscript.

ACKNOWLEDGMENTS

This work was funded by the Deutsche Forschungsgemeinschaft (DFG, German Research Foundation)-project number 267205415-CRC 1208 (subprojects A01: Sander H. J. Smits; A06: Daniel Degrandi, Klaus Pfeffer; A07: Birgit Strodel; and Z01: Kai Stühler) and DFG PF 259/8-2 Klaus Pfeffer, Daniel Degrandi. Wibke Schumann gratefully acknowledges funding received from the Jürgen Manchot Foundation (PhD fellowship). The Center for Structural Studies is funded by the DFG (FUGG project with grant number 417919780 and INST 208/761-1 to Sander H. J. Smits). Jennifer Loschwitz, Wibke Schumann, and Birgit Strodel gratefully acknowledge the Gauss Centre for Supercomputing e.V. (www.gauss-centre.eu) for funding this project by providing computing time on the GCS Supercomputer SuperMUC-NG at Leibniz Supercomputing Centre (www.lrz.de). Further computing time was granted through JARA-HPC (project JICS6A) on the supercomputer JURECA at the Forschungszentrum Jülich and by the Centre for Information and Media Technology at Heinrich Heine University Düsseldorf. Open Access funding enabled and organized by Projekt DEAL.

DATA AVAILABILITY STATEMENT

We uploaded the SAXS data to the Small Angle Scattering Biological Data Bank (SASBDB) (Kikhney et al., 2020; Valentini et al., 2014), with the accession code SASDLY9. The mass spectrometry proteomics data have been deposited to the ProteomeXchange Consortium via the PRIDE (Perez-Riverol et al., 2018) partner repository with the dataset identifier PXD026979. The MD trajectories are available from the authors upon request.

ORCID

Birgit Strodel https://orcid.org/0000-0002-8734-7765

REFERENCES

Abdullah N, Balakumari M, Sau A. Dimerization and its role in GMP formation by human guanylate binding proteins. Biophys J. 2010;99:2235–44.

Abraham MJ, Murtola T, Schulz R, Pàll S, Smith JC, Hess B, et al. GROMACS: high performance molecular simulations through multi-level parallelism from laptops to supercomputers. SoftwareX. 2015;1–2:19–25.

Abraham MJ, van der Spoel D, Lindahl E, Hess B, the GROMACS development team. GROMACS user manual version 2016.4. 2017.

Aliev AE, Kulke M, Khaneja HS, Chudasama V, Sheppard TD, Lanigan RM. Motional timescale predictions by molecular dynamics simulations: case study using proline and hydroxyproline sidechain dynamics. Proteins. 2014;82:195–215.

Bahadur RP, Zacharias M. The interface of protein-protein complexes: analysis of contacts and prediction of interactions. Cell Mol Life Sci. 2008;65:1059–72.

Baker N, Sept D, Joseph S, Holst M, McCammon J. Electrostatics of nanosystems: application to microtubules and the ribosome. Proc Natl Acad Sci U S A. 2001;98:10037–41.

Barz B, Loschwitz J, Strodel B. Large-scale, dynamin-like motions of the human guanylate binding protein 1 revealed by multiresolution simulations. PLoS Comput Biol. 2019;15:1–29.

Basu S, Wallner B. DockQ: a quality measure for protein-protein docking models. PloS One. 2016;11:1–9.

Berman HM, Westbrook J, Feng Z, Gilliland G, Bhat TN, Weissig H, et al. The Protein Data Bank. Nucleic Acids Res. 2000;28:235–42.

Best RB, Hummer G. Optimized molecular dynamics force fields applied to the helix-coil transition of polypeptides. J Phys Chem B. 2009;113:9004–15.

Bian X, Klemm RW, Liu TY, Zhang M, Sun S, Sui X, et al. Structures of the atlastin GTPase provide insight into homotypic fusion of endoplasmic reticulum membranes. Proc Natl Acad Sci U S A. 2011;108:3976–81.

Britzen-Laurent N, Bauer M, Berton V, Fischer N, Syguda A, Reipschläger S, et al. Intracellular trafficking of guanylate-binding proteins is regulated by heterodimerization in a hierarchical manner. PloS One. 2010;5:e14246.

Byrnes LJ, Sondermann H. Structural basis for the nucleotide-dependent dimerization of the large G protein atlastin-1/SPG3A. Proc Natl Acad Sci U S A. 2011;108:2216–21.

Chappie JS, Acharya S, Leonard M, Schmid SL, Dyda F. G domain dimerization controls dynamin's assembly-stimulated GTPase activity. Nature. 2010;465:435–40.

Chen Y, Zhang L, Graf L, Yu B, Liu Y, Kochs G, et al. Conformational dynamics of dynamin-like MxA revealed by single-molecule FRET. Nat Commun. 2017;8:15744.

Combe CW, Fischer L, Rappsilber J. xiNET: cross-link network maps with residue resolution. Mol Cell Proteomics. 2015;14:1137–47.

Cui W, Braun E, Wang W, Tang J, Zheng Y, Slater B, et al. Structural basis for GTP-induced dimerization and antiviral function of guanylate-binding proteins. Proc Natl Acad Sci U S A. 2021;118:e2022269118.

Daumke O, Praefcke GJK. Invited review: mechanisms of GTP hydrolysis and conformational transitions in the dynamin superfamily. Biopolymers. 2016;105:580–93.

Daumke O, Roux A, Haucke V. BAR domain scaffolds in dynamin-mediated membrane fission. Cell. 2014;156:882–92.

Daura X, Gademann K, Jaun B, Seebach D, van Gunsteren W, Mark A. Peptide folding: when simulation meets experiment. Angew Chem Int Ed. 1999;38:236–40.

Degrandi D, Konermann C, Beuter-Gunia C, Kresse A, Würthner J, Kurig S, et al. Extensive characterization of IFN-induced GTPases mGBP1 to mGBP10 involved in host defense. J Immunol. 2007;179:7729–40.

Degrandi D, Kravets E, Konermann C, Beuter-Gunia C, Klümpers V, Lahme S, et al. Murine guanylate binding protein 2 (mGBP2) controls *Toxoplasma gondii* replication. Proc Natl Acad Sci U S A. 2013;110:294–9.

Evans R, O'Neill M, Pritzel A, Antropova N, Senior A, Green T, et al. bioRxiv. 2021. https://doi.org/10.1101/2021.10.04.463034v1

Faelber K, Posor Y, Gao S, Held M, Roske Y, Schulze D, et al. Crystal structure of nucleotide-free dynamin. Nature. 2011;477:556–60.

Fattal DR, Ben-Shaul A. A molecular model for lipid-protein interaction in membranes: the role of hydrophobic mismatch. Biophys J. 1993;65:1795–809.

Ford MGJ, Chappie JS. The structural biology of the dynamin-related proteins: new insights into a diverse, multitalented family. Traffic. 2019;20:717–40.

Fröhlich C, Grabiger S, Schwefel D, Faelber K, Rosenbaum E, Mears J, et al. Structural insights into oligomerization and mitochondrial remodelling of dynamin 1-like protein. EMBO J. 2013;32:1280–92.

Gao S, Hu J. Mitochondrial fusion: the machineries in and out. Trends Cell Biol. 2021;31:62–74.

Ghosh A, Praefcke GJK, Renault L, Wittinghofer A, Herrmann C. How guanylate-binding proteins achieve assembly-stimulated processive cleavage of GTP to GMP. Nature. 2006;440:101–4.

Guinier A. Studies on transformation of *Escherichia coli* with plasmids. Ann Phys. 1939;12:161–237.

Humphrey W, Dalke A, Schulten K. VMD: visual molecular dynamics. J Mol Graph. 1996;14:33–8.

Ince S, Kutsch M, Shydlovskyi S, Herrmann C. The human guanylate-binding proteins hGBP-1 and hGBP-5 cycle between monomers and dimers only. FEBS J. 2017;284:2284–301.

Ince S, Zhang P, Kutsch M, Krenczyk O, Shydlovskyi S, Herrmann C. Catalytic activity of human guanylate-binding

protein 1 coupled to the release of structural restraints imposed by the C-terminal domain. FEBS J. 2020;288:febs.15348–599.

Jorgensen WL, Chandrasekhar J, Madura JD, Impey RW, Klein ML. Comparison of simple potential functions for simulating liquid water. J Chem Phys. 1983;79:926–35.

Jurrus E, Engel D, Star K, Monson K, Brandi J, Felberg LE, et al. Improvements to the APBS biomolecular solvation software suite. Protein Sci. 2018;27:112–28.

Kikhney AG, Borges CR, Molodenskiy DS, Jeffries CM, Svergun DI. SASBDB: towards an automatically curated and validated repository for biological scattering data. Protein Sci. 2020;29:66–75.

Kozakov D, Hall D, Xia B, Porter K, Olson A, Padhorny D, et al. The ClusPro web server for protein–protein docking. Nat Protoc. 2017;12:255–78.

Krapp C, Hotter D, Gawanbacht A, McLaren PJ, Kluge SF, Stürzel CM, et al. Guanylate binding protein (GBP) 5 is an interferon-inducible inhibitor of HIV-1 infectivity. Cell Host Microbe. 2016;19:504–14.

Krause D, Thörnig P. JURECA: modular supercomputer at Jülich Supercomputing Centre. J Large Scale Res Facil. 2018;4:A132.

Kravets E, Degrandi D, Ma Q, Peulen T-O, Klümpers V, Felekyan S, et al. Guanylate binding proteins directly attack *Toxoplasma gondii* via supramolecular complexes. Elife. 2016;5:e11479.

Kravets E, Degrandi D, Weidtkamp-Peters S, Ries B, Konermann C, Felekyan S, et al. The GTPase activity of murine guanylate-binding protein 2 (mGBP2) controls the intracellular localization and recruitment to the parasitophorous vacuole of *Toxoplasma gondii*. J Biol Chem. 2012;287:27452–66.

Kuhm T, de Agrela Pinto C, Gross L, Huber ST, Taisne C, Giannopoulou EA, et al. Structural basis of membrane targeting and coatomer assembly by human GBP1. bioRxiv. 2023. https://doi.org/10.1101/2023.03.28.534355

Legewie L, Loschwitz J, Steffens N, Prescher M, Wang X, Smits SH, et al. Biochemical and structural characterization of murine GBP7, a guanylate binding protein with an elongated C-terminal tail. Biochem J. 2019;476:3161–82.

Liberles DA, Teichmann SA, Bahar I, Bastolla U, Bloom J, Bornberg-Bauer E, et al. The interface of protein structure, protein biophysics, and molecular evolution. Protein Sci. 2012;21:769–85.

Lindenberg V, Mölleken K, Kravets E, Stallmann S, Hegemann JH, Degrandi D, et al. Broad recruitment of mGBP family members to *Chlamydia trachomatis* inclusions. PloS One. 2017;12:12.

Lindorff-Larsen K, Piana S, Palmo K, Maragakis P, Klepeis JL, Dror RO, et al. Improved side-chain torsion potentials for the Amber ff99SB protein force field. Proteins. 2010;78:1950–8.

Liu J, Noel JK, Low HH. Structural basis for membrane tethering by a bacterial dynamin-like pair. Nat Commun. 2018;9:3345.

Lorenz C, Ince S, Zhang T, Cousin A, Batra-Safferling R, Nagel-Steger L, et al. Farnesylation of human guanylate-binding protein 1 as safety mechanism preventing structural rearrangements and uninduced dimerization. FEBS J. 2020;287:496–514.

Loschwitz J, Steffens N, Wang X, Schäffer M, Pfeffer K, Degrandi D, et al. Domain motions, dimerization, and membrane interactions of the murine guanylate binding protein 2. Sci Rep. 2023;13:679.

Low HH, Löwe J. A bacterial dynamin-like protein. Nature. 2006;444:766–9.

Low HH, Sachse C, Amos LA, Löwe J. Structure of a bacterial dynamin-like protein lipid tube provides a mechanism for assembly and membrane curving. Cell. 2009;139:1342–52.

Madeira F, Park YM, Lee J, Buso N, Gur T, Madhusoodanan N, et al. The EMBL-EBI search and sequence analysis tools APIs in 2019. Nucleic Acids Res. 2019;47:W636–41.

Marqusee S, Baldwin R. Helix stabilization by Glu-...Lys+ salt bridges in short peptides of de novo design. Proc Natl Acad Sci U S A. 1987;84:8898–902.

McMahon HT, Gallop JL. Membrane curvature and mechanisms of dynamic cell membrane remodelling. Nature. 2005;438:590–6.

Morlot S, Galli V, Klein M, Chiaruttini N, Manzi J, Humbert F, et al. Membrane shape at the edge of the dynamin helix sets location and duration of the fission reaction. Cell. 2012;151:619–29.

Mukherjee S, Zhang Y. MM-align: a quick algorithm for aligning multiple-chain protein complex structures using iterative dynamic programming. Nucleic Acids Res. 2009;37:e83.

Negi SS, Braun W. Statistical analysis of physical-chemical properties and prediction of protein-protein interfaces. J Mol Model. 2007;13:1157–67.

Noel J, Noé F, Daumke O, Mikhailov A. Polymer-like model to study the dynamics of dynamin filaments on deformable membrane tubes. Biophys J. 2019;117:1870–91.

Notredame C, Desmond G, Jaap H. T-Coffee: a novel method for fast and accurate multiple sequence alignment. J Mol Biol. 2000;302:205–17.

Olszewski MA, Gray J, Vestal DJ. In silico genomic analysis of the human and murine guanylate-binding protein (GBP) gene clusters. J Interferon Cytokine Res. 2006;26:328–52.

Perez-Riverol Y, Csordas A, Bai J, Bernal-Llinares M, Hewapathirana S, Kundu DJ, et al. The PRIDE database and related tools and resources in 2019: improving support for quantification data. Nucleic Acids Res. 2018;47:D442–50.

Petoukhov MV, Svergun DI. Global rigid body modeling of macromolecular complexes against small-angle scattering data. Biophys J. 2005;89:1237–50.

Porter K, Padhorny D, Desta I, Ignatov M, Beglov D, Kotelnikov S, et al. Template-based modeling by ClusPro in CASP13 and the potential for using co-evolutionary information in docking. Proteins. 2019;87:1241–8.

Praefcke G, Kloep S, Benscheid U, Lilie H, Prakash B, Herrmann C. Identification of residues in the human guanylate-binding protein 1 critical for nucleotide binding and cooperative GTP hydrolysis. J Mol Biol. 2004;344:257–69.

Praefcke GJK, McMahon HT. The dynamin superfamily: universal membrane tubulation and fission molecules? Nat Rev Mol Cell Biol. 2004;5:133–47.

Prakash B, Praefcke G, Renault L, Wittinghofer A, Herrmann C. Structure of human guanylate-binding protein 1 representing a unique class of GTP-binding proteins. Nature. 2000;403:567–71.

PyMol. The PyMOL molecular graphics system, version 1.8. New York: Schrödinger, LLC; 2015.

Reubold T, Faelber K, Plattner N, Posor Y, Ketel K, Curth U, et al. Crystal structure of the dynamin tetramer. Nature. 2015;525:404–8.

Schulte K, Pawlowski N, Faelber K, Fröhlich C, Howard J, Daumke O. The immunity-related GTPase Irga6 dimerizes in a parallel head-to-head fashion. BMC Biol. 2016;14:1–8.

Shydlovskyi S, Zienert AY, Ince S, Dovengerds C, Hohendahl A, Dargazanli JM, et al. Nucleotide-dependent farnesyl switch orchestrates polymerization and membrane binding of human guanylate-binding protein 1. Proc Natl Acad Sci U S A. 2017; 114:E5559–68.

Sistemich L, Dimitrov Stanchev L, Kutsch M, Roux A, Günther Pomorski T, Herrmann C. Structural requirements for membrane binding of human guanylate-binding protein 1. FEBS J. 2021;288:4098–114.

Sistemich L, Kutsch M, Hämisch B, Zhang P, Shydlovskyi S, Britzen-Laurent N, et al. The molecular mechanism of polymer formation of Farnesylated human guanylate-binding protein 1. J Mol Biol. 2020;432:2164–85.

Steffens N, Beuter-Gunia C, Kravets E, Reich A, Legewie L, Pfeffer K, et al. Essential role of mGBP7 for survival of *Toxoplasma gondii* infection. MBio. 2020;11:11.

Stowell MH, Marks B, Wigge P, McMahon HT. Nucleotide-dependent conformational changes in dynamin: evidence for a mechanochemical molecular spring. Nat Cell Biol. 1999;1: 27–32.

Svergun D, Barberato C, Koch MHJ. *CRYSOL* – a program to evaluate X-ray solution scattering of biological macromolecules from atomic coordinates. J Appl Cryst. 1995;28:768–73.

Svergun DI, Petoukhov MV, Koch MH. Determination of domain structure of proteins from X-ray solution scattering. Biophys J. 2001;80:2946–53.

Taylor GA, Feng CG, Sher A. p47 GTPases: regulators of immunity to intracellular pathogens. Nat Rev Immunol. 2004;4:100–9.

Torchala M, Moal I, Chaleil R, Fernandez-Recio J, Bates P. SwarmDock: a server for flexible protein–protein docking. Bioinformatics. 2013;29:807–9.

Valentini E, Kikhney AG, Previtali G, Jeffries CM, Svergun DI. SASBDB, a repository for biological small-angle scattering data. Nucleic Acids Res. 2014;43:D357–63.

van Zundert G, Bonvin A. DisVis: quantifying and visualizing accessible interaction space of distance-restrained biomolecular complexes. Bioinformatics. 2015;31:3222–4.

Vöpel T, Syguda A, Britzen-Laurent N, Kunzelmann S, Lüdemann M-B, Dovengerds C, et al. Mechanism of GTPase-activity-induced self-assembly of human guanylate binding protein 1. J Mol Biol. 2010;400:63–70.

Warnock DE, Hinshaw JE, Schmid SL. Dynamin self-assembly stimulates its GTPase activity. J Biol Chem. 1996;271:22310–4.

Waterhouse AM, Procter JB, Martin DMA, Clamp M, Barton GJ. Jalview version 2—a multiple sequence alignment editor and analysis workbench. Bioinformatics. 2009;25:1189–91.

Wehner M, Kunzelmann S, Herrmann C. The guanine cap of human guanylate-binding protein 1 is responsible for dimerization and self-activation of GTP hydrolysis. FEBS J. 2012;279:203–10.

Weismehl M, Chu X, Kutsch M, Lauterjung P, Herrmann C, Kudryashev M, et al. Elucidating the activation mechanism for GBP1 oligomerization. bioRxiv. 2023.

Wolny M, Batchelor M, Bartlett G, Baker E, Kurzawa M, Knight P, et al. Characterization of long and stable de novo single alpha-helix domains provides novel insight into their stability. Sci Rep. 2017;7:44341.

Xavier A, Al-Zeer MA, Meyer TF, Daumke O. hGBP1 coordinates chlamydia restriction and inflammasome activation through sequential GTP hydrolysis. Cell Rep. 2020;31:107667.

Yan L, Sun S, Wang W, Shi J, Hu X, Wang S, et al. Structures of the yeast dynamin-like GTPase Sey1p provide insight into homotypic ER fusion. J Cell Biol. 2015;210:961–72.

Yu C, Zhao J, Yan L, Qi Y, Guo X, Lou Z, et al. Structural insights into G domain dimerization and pathogenic mutation of OPA1. J Cell Biol. 2020;219.

Zhu S, Bradfield CJ, Mamińska A, Park E-S, Kim B-H, Kumar P, et al. Cryo-ET of a human GBP coatomer governing cell-autonomous innate immunity to infection. bioRxiv. 2021.

Zimmerberg J, Kozlov MM. How proteins produce cellular membrane curvature. Nat Rev Mol Cell Biol. 2006;7:9–19.

SUPPORTING INFORMATION

Additional supporting information can be found online in the Supporting Information section at the end of this article.

How to cite this article: Schumann W, Loschwitz J, Reiners J, Degrandi D, Legewie L, Stühler K, et al. Integrative modeling of guanylate binding protein dimers. Protein Science. 2023; 32(12):e4818. https://doi.org/10.1002/pro.4818